NASA CR-72859
WANL-PR(VVV)-003
April, 1971

INVESTIGATION OF HIGH TEMPERATURE FRACTURE OF T-111 AND ASTAR-811C

By

R. E. Gold

Westinghouse Astronuclear Laboratory
Pittsburgh, Pennsylvania 15236

and

R. T. Begley

Westinghouse Research and Development Center
Pittsburgh, Pennsylvania 15235

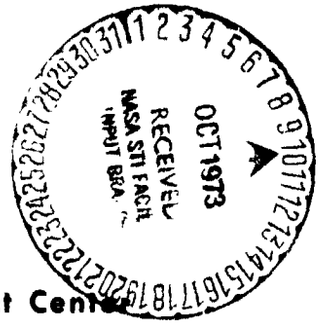

Prepared For

National Aeronautics And Space Administration
NASA Lewis Research Center
Task III of Contract NAS 3-11827
Paul Moorhead, Project Manager

NOTICE

This report was prepared as an account of Government-sponsored work. Neither the United States, nor the National Aeronautics and Space Administration (NASA), nor any person acting on behalf of NASA:

A.) Makes any warranty or representation, expressed or implied, with respect to the accuracy, completeness, or usefulness of the information contained in this report, or that the use of any information, apparatus, method, or process disclosed in this report may not infringe privately-owned rights; or

B.) Assumes any liabilities with respect to the use of, or for damages resulting from the use of, any information, apparatus, method or process disclosed in this report.

As used above, "person acting on behalf of NASA" includes any employee or contractor of NASA, or employee of such contractor, to the extent that such employee or contractor of NASA or employee of such contractor prepares, disseminates, or provides access to any information pursuant to his employment or contract with NASA, or his employment with such contractor.

Requests for copies of this report should be referred to:

National Aeronautics and Space Administration
Scientific and Technical Information Facility
P. O. Box 33
College Park, Maryland 20740

Astronuclear Laboratory

NASA CR-72859
WANL-PR(VVV)-003

FINAL REPORT

INVESTIGATION OF HIGH TEMPERATURE FRACTURE OF T-111 AND ASTAR-811C

by

R. E. Gold

WESTINGHOUSE ASTRONUCLEAR LABORATORY
Pittsburgh, Pennsylvania 15236

and

R. T. Begley

WESTINGHOUSE RESEARCH AND DEVELOPMENT CENTER
Pittsburgh, Pennsylvania 15235

prepared for

NATIONAL AERONAUTICS AND SPACE ADMINISTRATION

April, 1971

Task III of Contract NAS 3-11827

Fracture and Hot Crack Resistance of Welds in T-111 and ASTAR-811C

NASA Lewis Research Center
Cleveland, Ohio
Paul E. Moorhead, Project Manager
Materials and Structures Division

Astronuclear Laboratory

FOREWORD

This program was conducted by the Westinghouse Astronuclear Laboratory under NASA Contract NAS 3-11827. Mr. P. E. Moorhead of the NASA Lewis Research Center, Materials and Structures Division, was the NASA Project Manager for the program.

The objectives delineated and the results reported herein represent the requirements of Task III of Contract NAS 3-11827. Additional investigations which were performed as a part of this program are the subjects of additional reports. The final reports for this contract are the following :

Task	Title	Report Number
I	Influence of Restraint and Thermal Exposure on Welds in T-111 and ASTAR-811C	NASA CR-72858
II	The Varestraint Test for Refractory Metals	NASA CR-72828
III	Investigation of High Temperature Fracture of T-111 and ASTAR-811C	NASA CR-72859

Special appreciation and recognition are extended to Drs. R. A. Stickler and J. A. Cornie and Mr. C. W. Hughes of the Materials Department, Westinghouse Research and Development Center for their assistance with the transmission and scanning electron microscopy contained in this report.

TABLE OF CONTENTS

LIST OF ILLUSTRATIONS

LIST OF ILLUSTRATIONS (Continued)

LIST OF ILLUSTRATIONS (Continued)

LIST OF ILLUSTRATIONS (Continued)

LIST OF TABLES

ABSTRACT

The high temperature deformation and fracture behavior of T-111 and ASTAR-811C were studied over the temperature range 982° to 2205°C (1800° to 4000°F). As-cast and wrought-recrystallized material as well as GTA welds in sheet and plate were evaluated using conventional tensile and creep tests. Post-test examinations were performed using optical metallography, scanning electron microscopy and transmission electron microscopy.

A high temperature region of reduced ductility, in terms of tensile elongation, was identified for both alloys. The reduction in tensile elongation became more severe with increase in grain size, being near catastrophic for the as-cast specimens. Optical and electron metallography indicated that even for failures at very low total strain, considerable deformation of a very localized nature had occurred prior to fracture.

1.0 SUMMARY

Features of the deformation and fracture behavior of T-111 and ASTAR-811C were characterized over the temperature range 982° to 2205°C (1800° to 4000°F). Tensile and creep tests were used to test specimens prepared from as-cast and wrought-recrystallized material as well as from GTA sheet and plate welds. Post-test examinations were performed using optical metallography, scanning electron microscopy and transmission electron microscopy.

This investigation was prompted by recent observations of the high temperature mechanical behavior of T-111 which suggested premature intergranular failure may occur due to a drastic loss of ductility over a critical temperature range. ASTAR-811C was included in the program to permit assessment of the behavior of a more advanced, carbide strengthened alloy under the same conditions of testing. Testing as-cast and wrought-recrystallized specimens provided information on structural factors such as grain size while the inclusion of sheet and plate welds permitted some appreciation of the influence of microstructural heterogeneity. Estimates of the role of grain boundary sliding in the deformation process were inferred from observations of gage length fiducial line displacements occurring during creep testing.

A temperature range of reduced ductility, in terms of tensile elongation, was identified for both alloys. Although strain rate variations resulted in a shift of the "minimum ductility" temperature, for normal tensile strain rates it occurred at about 1649°C (3000°F). The width of the "trough" in the elongation vs. temperature relationship as well as the severity of impairment were related to the grain size, being increasingly severe with increasing grain size. The very fine grained wrought-recrystallized specimens did not, in fact, display a decrease in tensile elongation. However, post-test metallography indicated this merely reflected the greater number of grains in the cross section and that intergranular separation and cracking were quite severe.

Examination of the as-fractured specimens with scanning electron microscopy provided conclusive evidence that extensive deformation had occurred, even in those specimens where total tensile strains were virtually nil, but that all deformation appeared to have been concentrated in an extremely localized region adjacent to the grain boundaries. Transmission electron microscopy performed on several of the as-cast T-111 specimens revealed a general inability of the grain boundary regions to serve as barriers to dislocation slip at 1649°C (3000°F). Hence redistribution of strain to the grain volumes could not be achieved.

Qualitative differences in the deformation behavior of T-111 and ASTAR-811C were slight for tensile tests although the creep strength superiority of ASTAR-811C was apparent.

2.0 INTRODUCTION

This report presents the results of an investigation of the high temperature deformation and fracture behavior of the tantalum-base alloys T-111 (Ta-8W-2Hf) and ASTAR-811C (Ta-8W-1Re-0.7Hf-0.025C).

Recent observations of the high temperature mechanical behavior of T-111, as well as the behavior of grain boundary regions in multipass GTA plate welds, have suggested a possible ductility impairment occurs at some critical temperature range leading to pre nature intergranular failure. It was the purpose of this program, therefore, to investigate the factors controlling the high temperature deformation and fracture in this alloy, with particular attention being focused on the role of the grain boundary regions in the deformation process. ASTAR-811C was included in the program to permit assessment of the behavior of a more advanced, carbide strengthened alloy under the same conditions of testing.

The program was designed to provide information on the influence of such structural factors as grain size and process history by testing as-cast and wrought-recrystallized material in addition to including tests on GTA sheet and plate welds where chemical and microstructural heterogeneities might be influential. The bulk of the testing was performed using conventional tensile tests, with the as-cast material being tested at five temperatures ranging from 1205° to 1982°C (2200° to 3600°F) using a variety of strain rates covering the range 0.005 $min.^{-1}$ through 2.0 $min.^{-1}$. Tensile tests on the other forms were confined to testing at 1427°, 1649° and 1816°C (2600°, 3000° and 3300°F) at the "normal" 0.05 $min.^{-1}$ strain rate.

The known importance of grain boundaries in creep deformation at elevated temperatures and their implied importance in the deformation and fracture of T-111 in the preceding phases of this program dictated the inclusion of a series of creep tests in the experimental evaluation. The purpose of these tests was to provide information regarding the probable role of grain boundary sliding as a deformation and/or fracture mode at the temperatures of interest.

Optical metallography, scanning electron microscopy and transmission electron microscopy were utilized to facilitate interpretation of the test results.

3.0 TECHNICAL PROGRAM

3.1 Test Program

The experimental program, outlined in Figure 1, was designed to permit evaluation of the relative importance of several of the metallurgical factors which might reasonably be contributing to the observed behavior. The initial task of the program was aimed at determining, by experimental measurement, the range of temperatures to which the first deposited passes of a multipass GTA plate weld are exposed during subsequent deposition of later filler passes. The results of these measurements were used to aid in selection of test temperatures for later experimental tasks.

The first, and most extensive, phase of the tensile testing was performed on round bar specimens of as-cast T-111 and ASTAR-811C. Testing was conducted at 1205°, 1427°, 1649°, 1816°, and 1982°C (2200°, 2600°, 3000°, 3300°, and 3600°F) using strain rates of 0.005 (or 0.05), 0.5 and 2.0 min^{-1} at each temperature.

Based on these results the temperature-strain rate conditions used for the tensile testing of wrought-recrystallized and single pass GTA sheet weld specimens were selected. Testing on both of these specimen types was performed at 1427°, 1649°, and 1816°C (2600°, 3000°, and 3300°F) at a strain rate of 0.05 min^{-1}.

In an effort to evaluate the role of grain boundary sliding in the deformation and fracture behavior of GTA sheet welds of T-111 and ASTAR-811C, single pass GTA sheet welds were tested using both creep and conventional tensile test methods. Tensile tests were performed at a strain rate of 0.005 min^{-1} at 982°, 1205°, 1427°, 1538°, 1760°, and 1982°C (1800°, 2200°, 2600°, 2800°, 3200°, and 3600°F) on specimens whose gauge lengths had been mechanically polished and lightly scribed with a grid. Creep tests were performed on similarly prepared GTA sheet weld specimens at 1316°, 1427° and 1538°C (2400°, 2600°, and 2800°F) in ultra-high vacuum ($< 1.33 \times 10^{-6}$ N/m^2 ($< 10^{-8}$ torr) pressure). Following

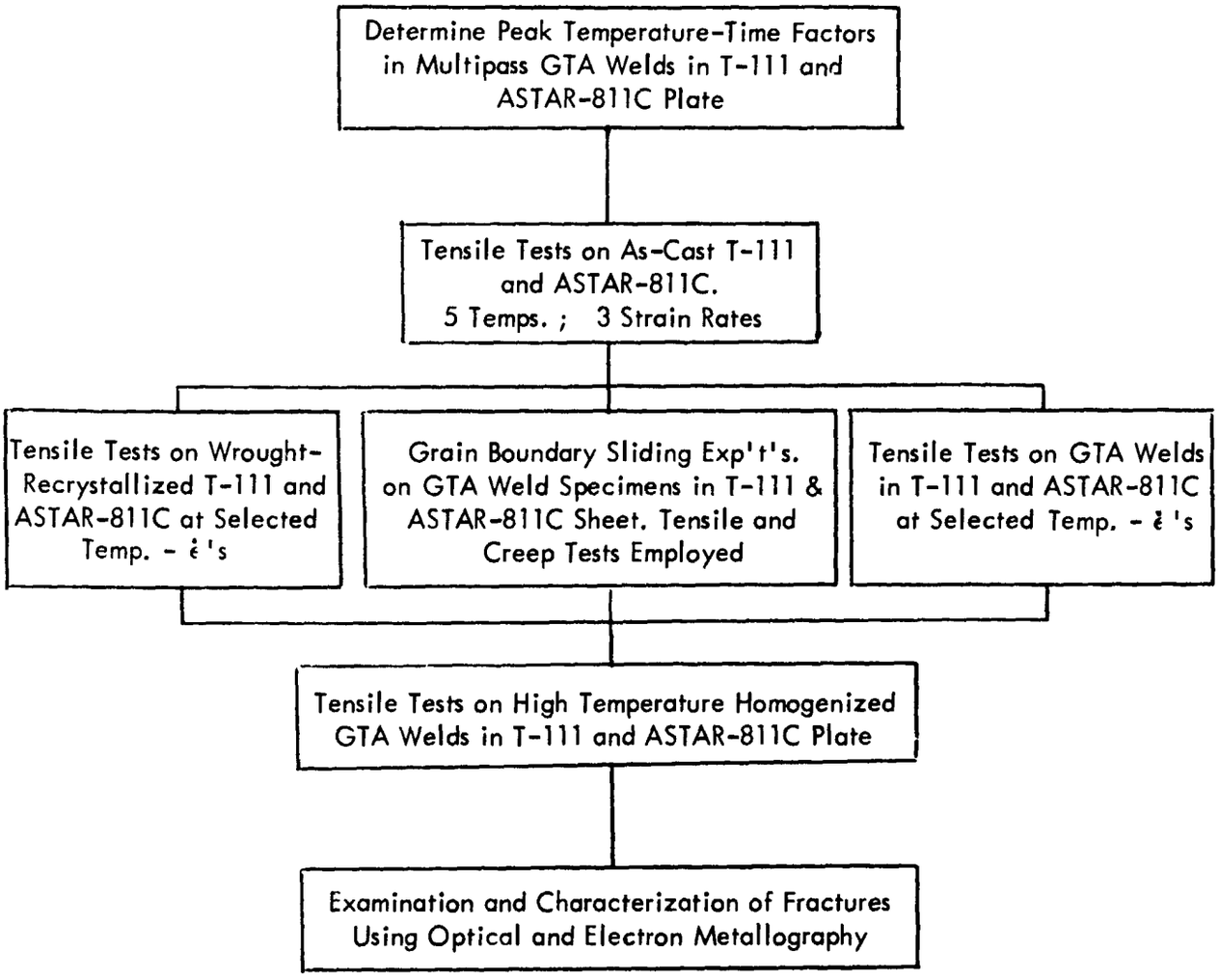

FIGURE 1 - Outline of Test Program for T-111 and ASTAR-811C.

both tensile and creep testing the specimens were examined microscopically to establish, by means of noting the displacement of grid markers where they cross grain boundaries, some estimate of the contribution of grain boundary sliding to total deformation strain.

The final phase of the testing program was directed toward evaluating the effectiveness of very high temperature homogenization annealing in alleviating the propensity for intergranular failure at low total strain. Tensile specimens were machined from plate welds of T-111 and ASTAR-811C. Identical specimens of each alloy were tested at 1649°C (3000°F) in the as-welded condition and after a 1 hour - 2483°C (4500°F) post-weld homogenization anneal.

Optical and electron metallographic techniques were used extensively to aid in the interpretation of the test results. In particular, scanning electron microscopy was employed to examine and characterize the topology of the fracture surfaces.

3.2 Procedures

Welding Procedures

The gas-tungsten-arc (GTA) welding process was used exclusively for all plate and sheet welding. All welding was performed in a vacuum purged weld chamber using an ultra-high purity helium atmosphere. The weld atmosphere was continuously monitored for oxygen and water vapor contents during all welding operations. For the bead-on-plate sheet welding the oxygen and water vapor were maintained at less than 5 ppm by volume whereas for the greater heat input plate welding the maximum level was set as 10 ppm by volume. All welding was done using straight polarity direct current (SPDC).

All bead-on-plate sheet welds in both T-111 and ASTAR-811C 0.152 cm (0.060 in.) sheet were made using the following welding parameters ;

Weld Current	200 amps
Weld Speed	38.1 cm/min (15 in/min)
Arc Gap	0.157 cm (0.062 inches)

Electrodes were made of 0.236 cm (3/32 inch) diameter centerless ground 2% thoriated tungsten which had been ground to a blunted tip. Welding was done semi-automatically using a traversing table which permitted a uniform, reproducible travel speed of the workpiece relative to the electrode. All sheet welds were inspected for basic quality using visual, dye penetrant and radiographic techniques.

The multipass GTA plate welds in 0.952 cm (0.375 in.) thick T-111 and ASTAR-811C were prepared using manual feed of 0.203 cm (0.080 inch) diameter filler wire at a uniform welding speed of 25.4 cpm (10 ipm). The plate weld joint design which was used is shown in Figure 2.

Tensile Testing

Tensile specimens were of two configurations. Round bar specimens, Figure 3, were used for as-cast, wrought-recrystallized, and GTA plate weld specimens. The specimens used for the tests on 0.152 cm (0.060 inch) sheet welds were machined to the configuration shown in Figure 4. Details of the strain rates employed for the various tests will be deferred to the appropriate Results section of this report. All elevated temperature tests were performed at pressures $< 1.33 \times 10^{-3}$ N/m^2 ($< 10^{-5}$ torr). Specimen gage sections were wrapped in tantalum foil for additional contamination protection during testing.

Creep Testing

All creep tests were performed on specimens machined from single pass GTA sheet welds. The specimen configuration used in all cases is that shown in Figure 5. All tests were conducted in sputter ion pumped ultra-high vacuum creep systems. Pressures were maintained $< 1.33 \times 10^{-6}$ N/m^2 ($< 10^{-8}$ torr) throughout testing. Details of test temperatures and stresses are reported in the appropriate Results section of this report.

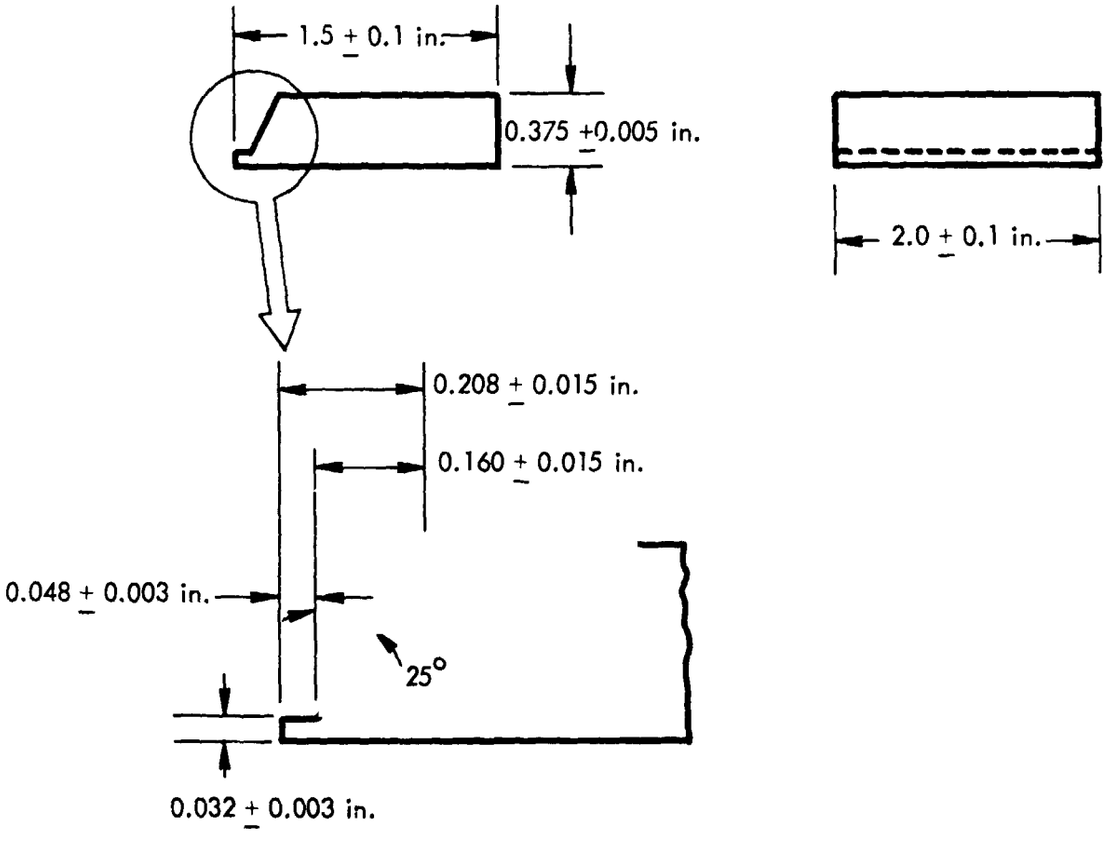

FIGURE 2 - Butt Joint Configuration Used for Plate Welds.

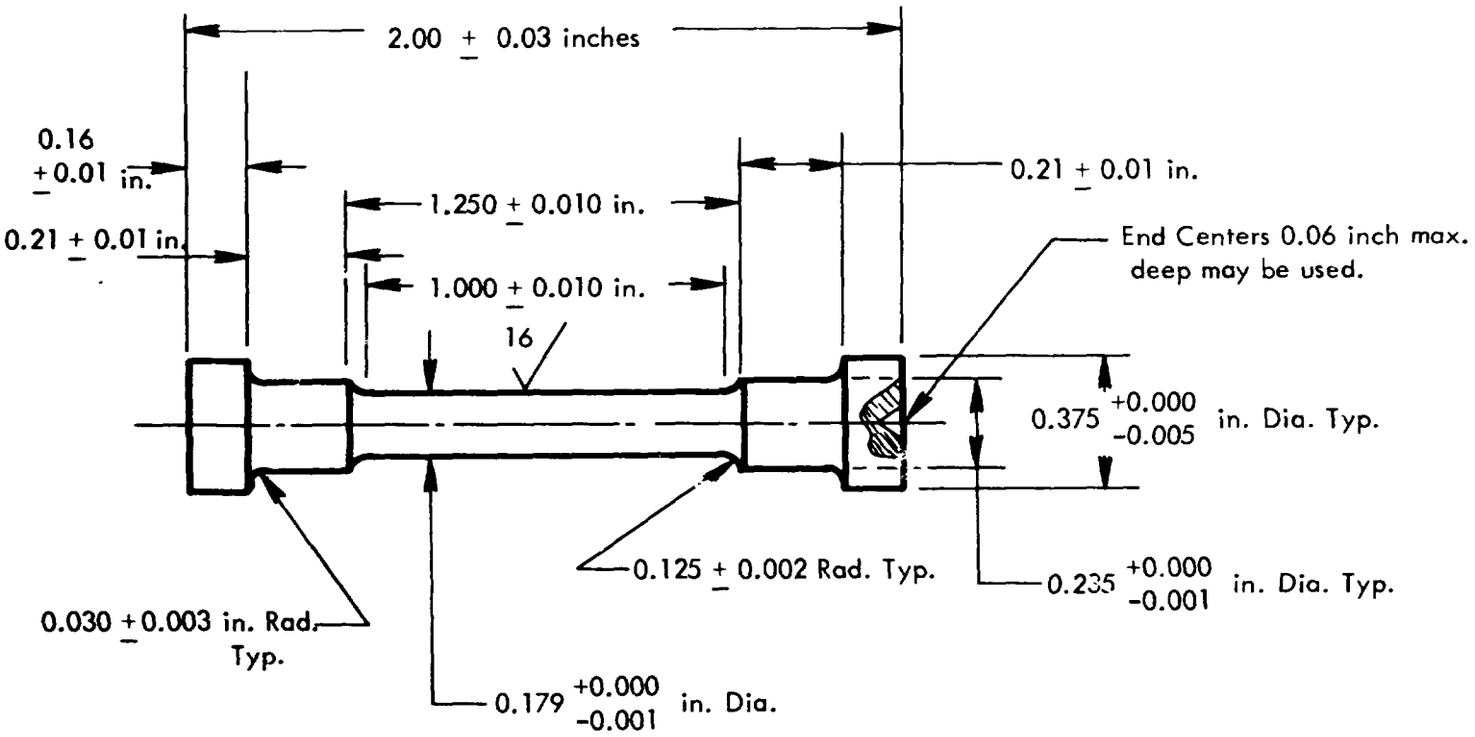

FIGURE 3 - Round Bar Tensile Specimen Configuration Used for T-111 and ASTAR-811C This Program.

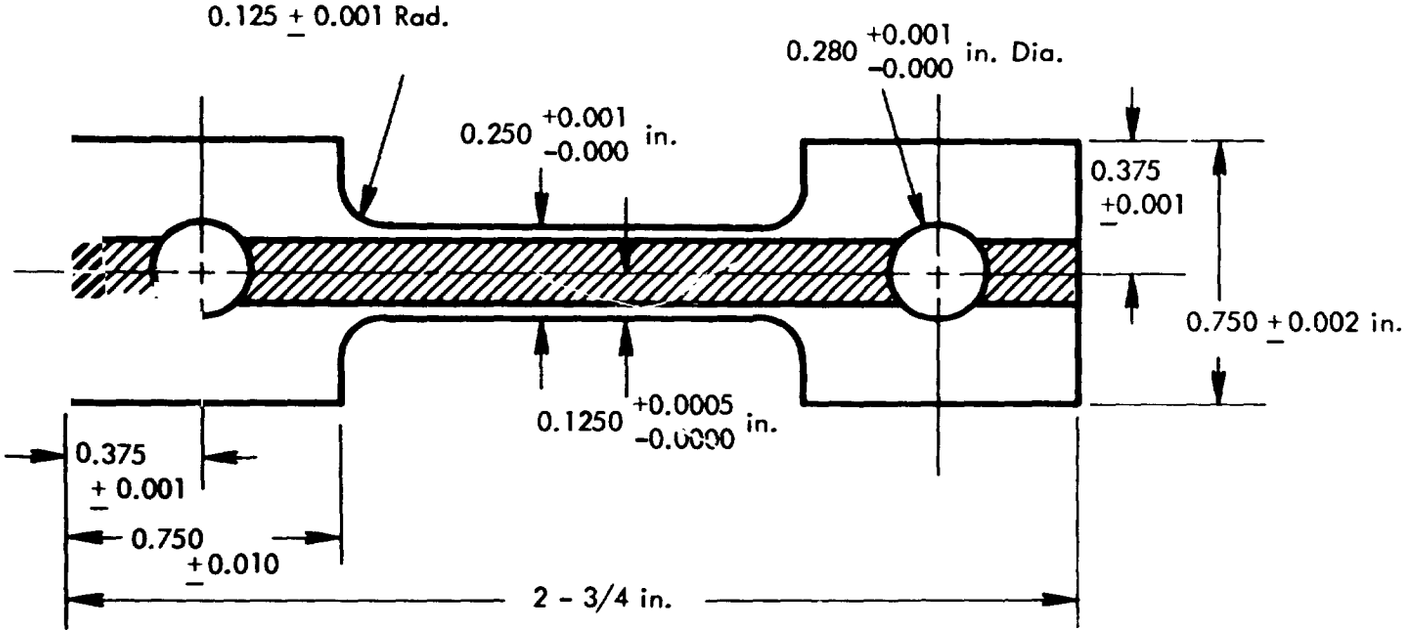

FIGURE 4 - Specimen Configuration Used for Tensile Tests on T-111 and ASTAR-811C GTA Sheet Welds.

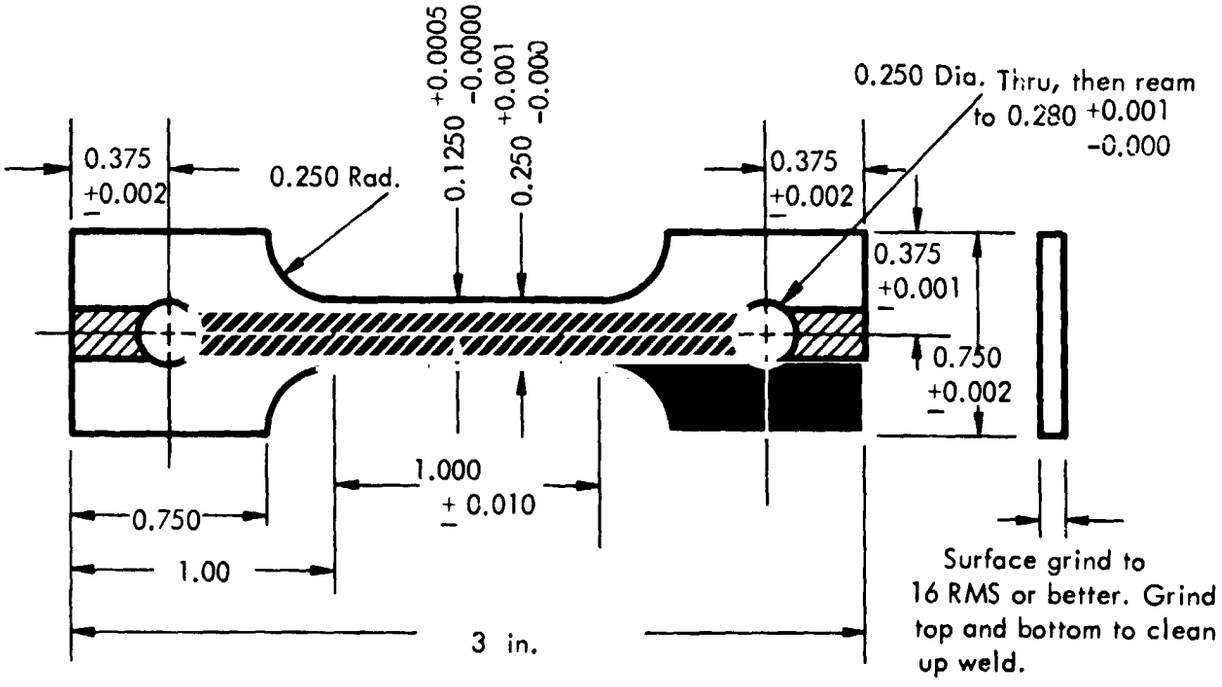

FIGURE 5 - Specimen Configuration Used for Creep Tests on T-111 and ASTAR-811C GTA Sheet Welds.

Scanning Electron Microscopy

Examination and characterization of fracture surfaces was accomplished using the Cambridge Stereoscan-Mark IIa scanning electron microscope located at the Westinghouse Research and Development Center. In addition to its basic scanning function this instrument is equipped to provide for energy-dispersive x-ray spectrography as well as for the recording of electron channeling patterns from selected surface areas (smaller than 5 microns in diameter, from a surface layer less than several hundred angstrom units thick). This instrument therefore provides the unique capability of recording surface features, surface composition and crystallographic details of the identical area of a specimen.

The excellent depth of focus and resolution of the scanning electron microscope eliminated the necessity for specimen preparation, thereby allowing immediate and direct observation of the fracture surfaces.

Transmission Electron Microscopy

Thin foils were prepared from selected T-111 specimens and examined using the Philips EM-300 transmission electron microscope located at the Westinghouse Research and Development Center. The foils were prepared by mechanically polishing specimens to a thickness of about 0.010 cm, then electropolishing at room temperature in an electrolyte of 85 H_2SO_4-15HF to breakthrough.

3.3 Program Materials

3.3.1 T-111

The T-111 used for this evaluation was furnished by NASA-Lewis from material remaining from Contract NAS 3-10602 (Development of Large Diameter T-111 Tubing). For that program a 1061 kg (2340 lb) T-111 ingot, the largest single tantalum-base alloy ingot ever produced, was prepared by a combination of electron beam and consumable vacuum arc melting. Detailed description of the processing of this material has been reported elsewhere[1].

Specific details regarding the location and history of the various individual specimen types will be presented in a later section of this report. Chemical analyses of the as-cast ingot are presented in Table 1.

3.3.2 ASTAR-811C

To provide sufficient material for this program and companion Tasks of this contract[2,3], ASTAR-811C was produced in a commercial size ingot for the first time. A 137.9 kg (304 lb) ingot was prepared by Wah Chang Corporation of Albany, Oregon using double vacuum-arc melting practice. The 18.4 cm (7-1/4 inch) diameter ingot was canned in molybdenum and extruded at 1649°C (3000°F) using a 3:1 extrusion ratio. The machined ingot and molybdenum extrusion can are shown prior to assembly in Figure 6. Following extrusion and cleanup the usable yield, weighing 110.6 kg (244 lbs), was annealed 1 hour at 1649°C (3000°F), then forged to sheet bar at 1260°C (2300°F). After cleanup the as-forged sheet bar was processed to plate, sheet and wire as required to satisfy the testing requirements of the experimental program.

Metallurgical data and chemical analyses of the as-received material are presented in Tables 2 and 3, respectively. Also shown in Table 3 are the analyzed chemistry values for the original development heat of ASTAR-811C produced at the Astronuclear Laboratory under Contract NAS 3-2542[4]. The slightly higher W and Re contents of the program heat (Heat 650078) suggested the desirability of characterizing the base metal mechanical properties of this material. Base metal tensile properties were determined at -196°, RT, 1205°, 1649° and 1982°C (-320°, RT, 2200°, 3000° and 3600°F) using 0.089 cm (0.035 inch) thick sheet specimens. These results are presented in Table 4 along with the data for comparable tests conducted under NAS 3-2542. The program heat is seen to be somewhat stronger than the development heat, particularly at the lower test temperatures, although the ductility, measured in terms of the tensile elongation, is quite similar. It bend tests (33% outer fiber strain) indicated a bend DBTT of -157°C (-250°F) for Heat 650078 as compared to < -196°C (< -320°F) for the development heat. The high yield and ultimate tensile strength is likely

TABLE 1 - Chemical Analyses of As-Melted T-111 Ingot.

Ingot Location[a]	Wah Chang Analysis[b]					Westinghouse Analysis[b]				
	W	Hf	C	O	N	W	Hf	C	O	N
Top (surface)	8.1	2.05	40	70	25	--	---	--	--	--
Top (interior)	7.9	2.35	--	--	--	7.8	2.16	16	15	18
Center (surface)	7.9	1.95	40	--	27	--	---	--	--	--
Center (interior)	--	--	--	--	--	7.9	1.98	16	23	--
Bottom (surface)	8.3	1.95	40	60	29	--	---	--	--	--
Bottom (interior)	8.5	1.75	50	--	5	8.2	1.68	12	21	5

(a) Refers to position along the length of the 42 inch (106.7 cm.) long, 10 inch (25.4 cm.) diameter ingot.

(b) Metal analyses in w/o ; interstitial analyses in wt. ppm.

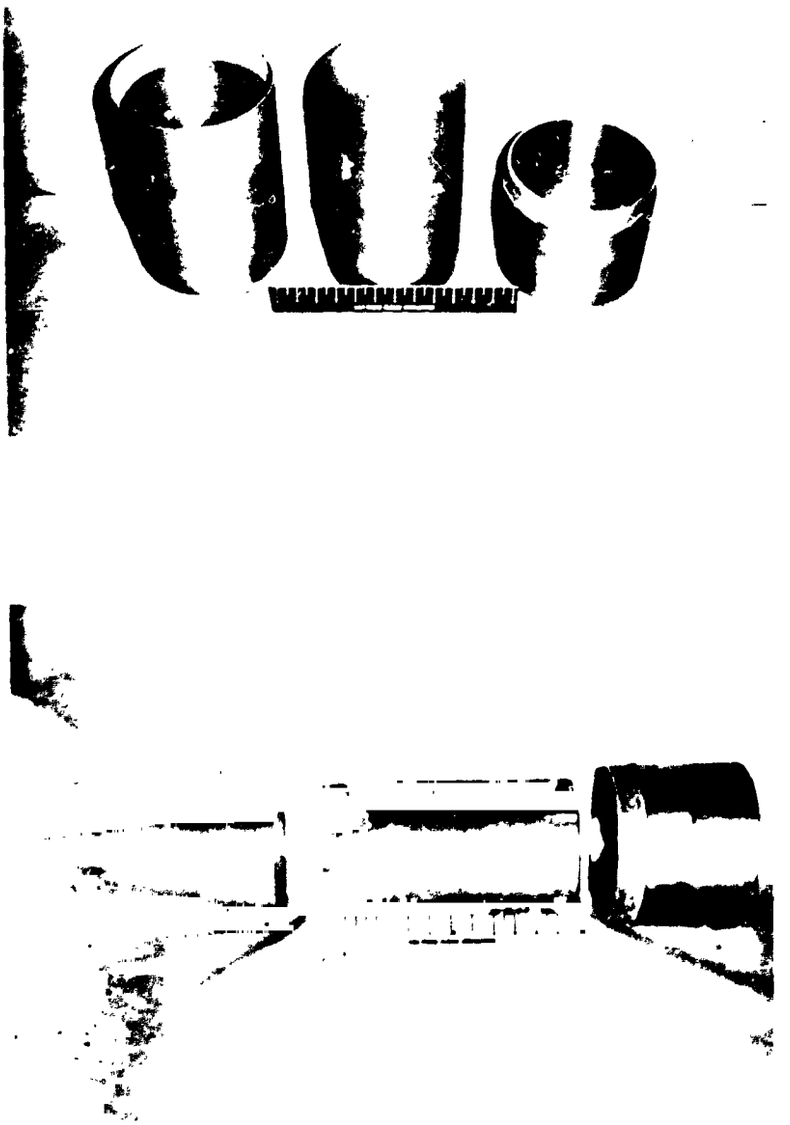

FIGURE 6 - ASTAR - 811C Ingot and Molybdenum Container Prior to Assembly for Extrusion.

Form	Hardness[a]		Grain Size		Used For
	Kg/mm^2	$10^7 N/m^2$	ASTM	Avg. Dia., μm.	
0.035 in(0.089 cm.) Sheet	276	270	8.5	19	bend ductility[b]
0.220/0.375 inch (0.559/ 0.952 cm.) Plate	---	---	8.5	22	plate weld studies [b]
0.125 in.(0.318 cm.) Plate	283	277	9.5	13	Varestraint [c]
0.035 in. (0.089 cm.) Sheet	281	275	9.5	13	Fracture studies

(a) 10 Kg (98.06 N) load used for hardness determinations.

(b) Subject of Task I ; see Reference (2).

(c) Subject of Task II ; see Reference (3).

TABLE 2 - Metallurgical Data for As-Received ASTAR-811C (Heat 650078).

Form	Certified Analysis [a]							Check Analysis [a]		
	Re	Ta	W	Hf	C	O	N	C	O	N
0.220/0.375 inch (0.559/0.952 cm) Plate	1.39	Bal	8.1	0.9	245	50	12	240	10	10
0.125 inch(0.318 cm) Plate	1.39	Bal	8.1	0.9	230	75	15	210	10	10
0.035 inch(0.089 cm) Sheet	1.39	Bal	8.1	0.9	250	50	12	230	10	12
Original Development Heat [b]	0.98	Bal	7.3	0.86	200	13	20		-	-

(a) Metal analyses in w/o; C,O,N, analyses in wt. ppm.

(b) Original development heat data from Reference (4).

TABLE 3 - Chemical Analysis of As-Received ASTAR-811C (Heat 650078).

Heat (a)	Test Temp.		UTS		0.2% Y.S.		% Elongation	
	°F	°C	ksi	10^7 N/m^2	ksi	10^7 N/m^2	Unif.	Total
650078	- 320	- 196	182.9	126.1	166.5	114.8	18.2	24.9
3-2542	- 320	- 196	165.3	114.0	147.7	101.8	22.1	26.3
650078	RT	RT	117.5	81.0	98.1	67.6	15.3	27.3
3-2542	RT	RT	104.0	71.7	85.0	58.6	16.4	26.6
650078	2200	1205	58.8	40.5	36.3	25.0	15.4	29.1
3-2542	2200	1205	49.9	34.4	31.6	21.8	--	28.8
650078	3000	1649	23.5	16.2	22.1	15.2	1.4	87.4
3-2542	2800	1538	28.4	19.6	23.0	15.8	--	49.5
650078	3600	1982	10.3	7.1	10.1	7.0	0.6	112.7

(a) Heat 650078 used this program.

Original development heat referenced as 3-2542 ; see Reference (4).

A constant 0.05 min^{-1} strain rate used throughout all tests.

TABLE 4 - Comparative Tensile Properties for Program ASTAR-811C and Original Development Heat.

due to the slightly higher tungsten and rhenium contents. Rhenium, in particular, has been observed to be a potent solid solution strengthener at low temperatures when present in the tantalum matrix[5]. The relevance of the difference in materials is discussed later in the appropriate Results section of this report.

4.0 RESULTS

The purpose of this section is to present the test data obtained during the performance of the experimental program. Other data pertinent to the evaluation of these data are also presented. These include pre- and post-test metallography, hardness determinations, and the results of examinations of the fracture surfaces with scanning electron microscopy. The general discussion of these results is deferred to the DISCUSSION section of this report.

4.1 Temperature-Time Profile Determinations in Plate Welds

The temperature-time profiles encountered during multipass GTA welding of 0.952 cm (3/8 inch) T-111 plate were determined by measuring the output of thermocouples, embedded in the base region of plate welds, during deposition of subsequent filler passes. A review of the specific process history of the welds used for this purpose follows:

a) 3 T-111 0.952 cm (3/8 inch) plate specimens were machined for welding. Weld joint design shown in Figure 2 was used.

b) A root (centerline fusion) pass and 2 filler passes were completed.

c) Holes were drilled from the underside of the plates to a depth which would allow the thermocouple beads to be placed about 0.254 cm (0.10 inch) below the weld surface. Details of the weld joint-thermocouple geometry are shown in Figure 7. The thermocouples were located so as to be in regions of severe grain boundary cracking.

d) W vs W/26Re thermocouples, encased in tantalum sheaths and insulated by beryllia powder, were placed in the drilled holes.

e) The plate welds, designated B1, B2 and B3, were then completed using as many additional filler passes as required to fill the weld joint. The temperature-time profiles were recorded directly for each of the thermocouples in a particular weld joint on separate Speedomax G strip-chart recorders.

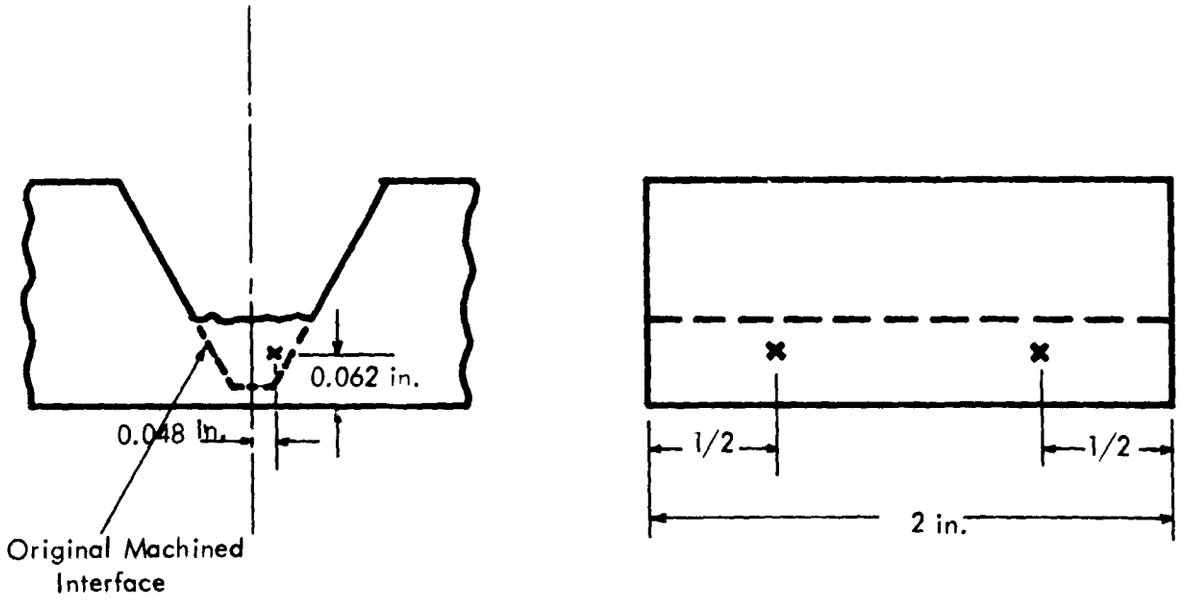

FIGURE 7 - Weld Joint-Thermocouple Geometry Used for Time-Temperature Measurements in Plate Welds.

f) Following welding the various welds were sectioned to determine the location and incidence of grain boundary cracking.

The thermal records obtained for plate welds B1, B2 and B3 are summarized in Tables 5, 6 and 7, respectively, in terms of heat input and peak temperature obtained. A plot of the temperature vs. time data for one of the thermocouples used in plate weld B1 is shown in Figure 8. The general shape of these curves is typical of thermocouple records made at points very near fusion zones in plate welds[6,7,8].

The mathematics of conduction from moving heat sources has been treated in classical works on heat conduction[9,10] and, with the establishment of certain idealized boundary conditions, solutions presented can be applied quite realistically to the field of welding. Adams[6] has discussed some of the more difficult problems encountered in trying to obtain metallurgically useful information from such solutions and has demonstrated a reasonable degree of success can be attained so long as one properly defines the obtaining heat flow conditions. One might therefore argue for the calculation, rather than the experimental determination, of the temperatures of interest. However, for the present program several factors complicate a purely mathematical approach to the point of extreme difficulty. These include:

- Irregularities in weld filler metal deposition rate due to the manual weld techniques employed.
- The limited specimen size would necessitate further modifications of the already idealized boundary conditions of the mathematical solutions.
- The extremely high melting point, and hence weld metal deposition temperature, of tantalum base alloys indicates heat losses by radiation probably constitute the major source of heat loss to temperatures as low as 816°C (1500°F). Normal heat conduction equations (and their solutions), by definition, do not provide a means for taking this into account.

Weld Pass No.	Approx. Weld Time (secs.)	E (volts)	I (amps.)	Power (kwatts)	Heat Input (kjoules/cm.)	Peak Temperatures*			
						TC 4		TC 5	
						°F	°C	°F	°C
1	21	20	272	5.44	22.5	3870	2132	3335	1835
2	19	22	296	6.51	24.4	3655	2013	--	--
3	19	22	308	6.78	25.4	3300	1815	--	--
4	16	24	325	7.80	24.6	3180	1749	--	--
5	21	23	318	7.31	30.2	3205	1763	2425	1329
6	15	22.5	298	6.70	19.8	2870	1576	2145	1174
7	17	25	309	7.72	25.9	2950	1621	2270	1243

* TC 3 was near the finishing end of weld. TC 4 was near starting end of weld.

No set time interval observed between weld passes; the only criterion was to let the weld cool to "black heat".

TC 3 was inaccurately positioned in the drilled hole; hence, temperatures recorded were consistently 500 to 800°F (260 to 427°C) lower than those of TC 4.

No signal was detected from TC 3 on several weld passes. Subsequent examination revealed a possible break in one of the TC wires, apparently caused by the mismatch in thermal expansion between the wires and the beryllia insulation.

TABLE 5 - Weld Joint B1 , Thermal Record.

Weld Pass No.	Approx. Weld Time (secs.)	E (volts)	I (amps.)	Power (kwatts)	Heat Input (kjoules/cm.)	Peak Temperatures *			
						TC 2		TC 1	
						°F	°C	°F	°C
1	26	20	280	5.60	28.7	3605	1985	3660	2016
2	26	21	280	5.88	30.1	3245	1785	3255	1791
3	29	21.5	295	6.34	36.2	3075	1690	3360	1849
4	24	21	293	6.15	29.0	2850	1566	2875	1579
5	29	20	288	5.76	32.9	2740	1504	3065	1685
6	19	22	300	6.60	24.7	2635	1446	2675	1468
7	20	25.5	312	7.96	31.3	2850	1566	3025	1663

* TC 1 was near the finishing end of the weld. TC 2 was near the starting end of the weld.

Five minute interpass time allowed between successive weld passes.

TABLE 6 - Weld Joint B2, Thermal Record.

Weld Pass No.	Approx. Weld Time (secs.)	E (volts)	I (amps.)	Power (kwatts)	Heat Input (kjoules/cm.)	Peak Temperatures *			
						TC 5		TC 6	
						°F	°C	°F	°C
1	16	23	315	7.24	22.8	3240	1782	3375	1857
2	14.5	25	320	8.00	22.8	2905	1596	3165	1740
3	15	25	330	8.25	24.4	2960	1627	3095	1702
4	14.8	25	315	7.88	22.9	2770	1521	2805	1540
5	19	23	300	6.90	25.8	2790	1532	2600	1427
6	16	24	300	7.20	22.7	2505	1374	2515	1380
7	19	22	290	6.38	23.8	2505	1374	2375	1302
8	19	26	290	7.54	28.3	2815	1546	2510	1377

* TC 5 was near the finishing end of the weld. TC 6 was near the starting end of the weld.

Five minute interpass time allowed between successive weld passes.

TABLE 7 - Weld Joint B3 , Thermal Record.

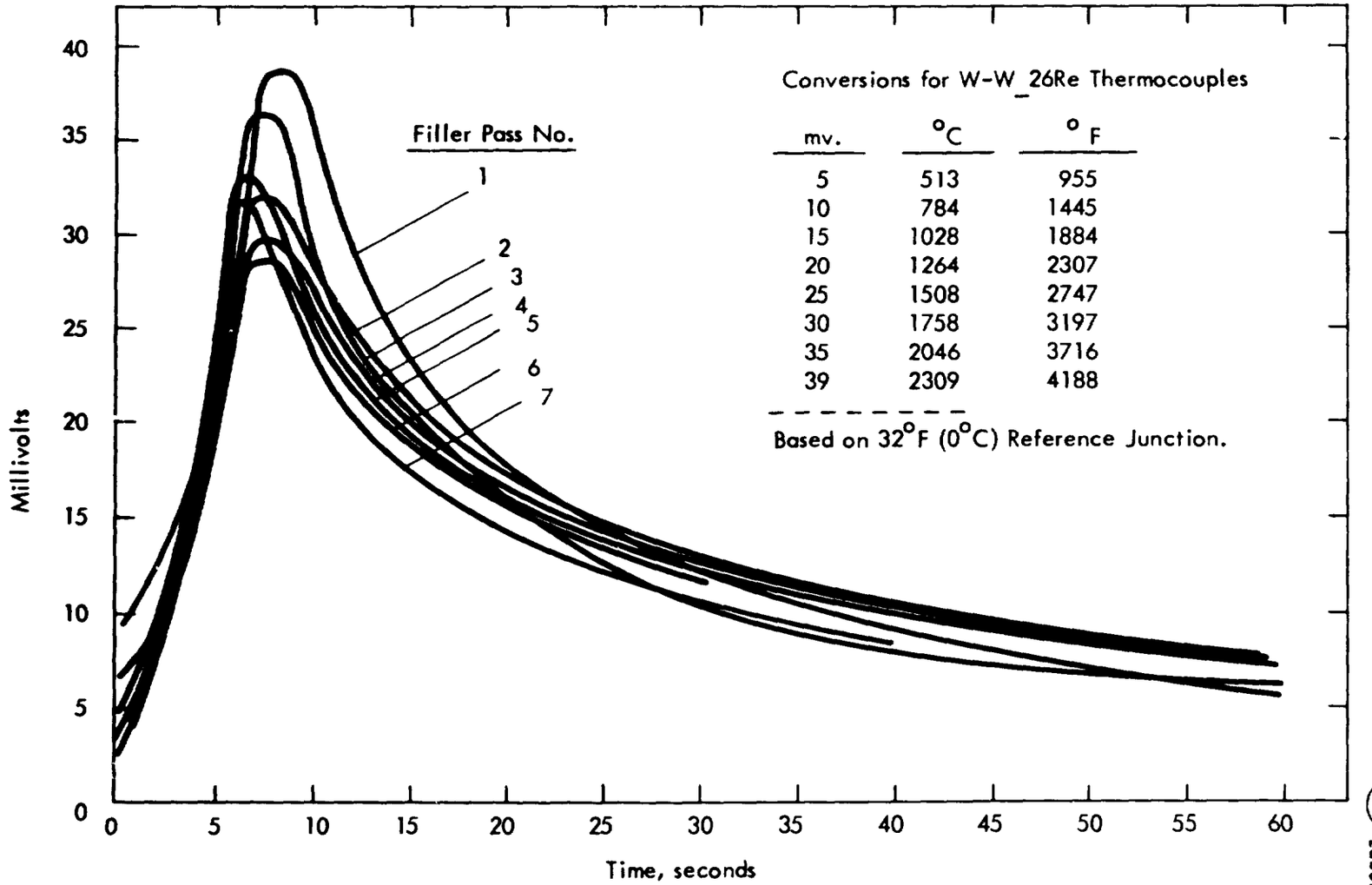

FIGURE 8 – Plot of Temperature–Time Data for Plate Weld B1 (See Table 5).

The data of Tables 5, 6 and 7 indicate the peak temperature in the regions most severely affected by grain boundary underpass cracking ranges from 1371°C (2500°F) to just over 1982°C (3600°F). The high temperature tensile tests on GTA sheet welds in T-111 and ASTAR-811C indicated a ductility minimum, in terms of total elongation at fracture, exists within this range of temperatures. This temperature range is consistent with the physical metallurgy of those processes which would be expected to reduce the importance of stress concentrations at the grain boundaries. At lower temperatures work-hardening should occur more uniformly throughout the matrix and regions adjacent to the grain boundaries while at higher temperatures the ease with which dynamic softening processes or grain boundary migration occur should alleviate the tendency for formation and propagation of grain boundary cracks.

As a result of the temperature-time measurements, test temperatures for the as-cast T-111 and ASTAR-811C specimens were placed in the temperature range 1205° through 1982°C (2200° through 3600°F), inclusive.

4.2 Tensile Testing

Tests were conducted on T-111 and ASTAR-811C specimens representing a variety of metallurgical conditions. The initial, and most extensive, evaluation was conducted using specimens prepared from as-cast material. In addition, tests were conducted on wrought-recrystallized rod, single pass GTA welded 0.152 cm (0.060 inch) sheet, and specimens machined from multipass GTA plate welds in 0.952 cm (3/8 inch) thick plate.

The initial microstructure of each of these material forms are shown in Figures 9 through 12. The average grain size and Vickers hardness were determined to be as follows:

23,201 Grain Size 0.72 mm. 50X
DPH 190

T-111

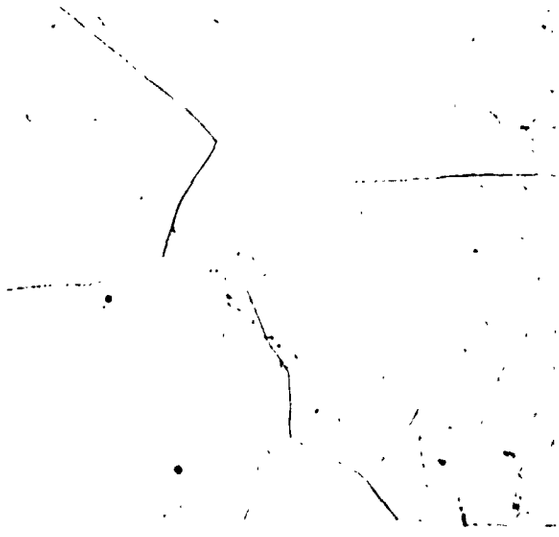

23,202 Grain Size 0.8 - 1.2 mm. 50X
DPH 284

ASTAR-811C

FIGURE 9 - Pre-Test Microstructure of As-Cast T-111 and ASTAR-811C.

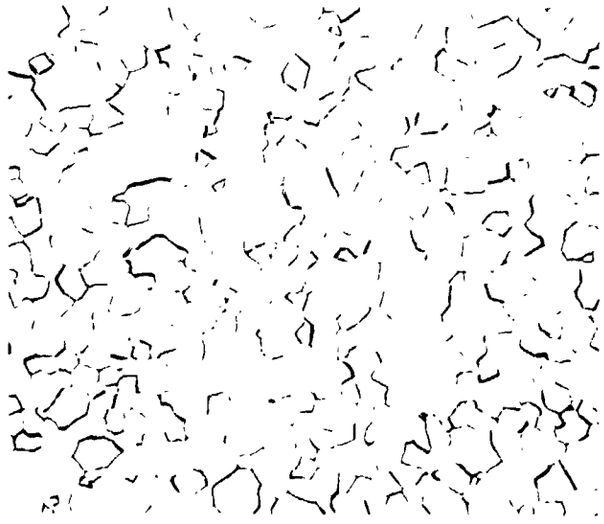

23,171 Grain Size 0.029 mm. 100X
DPH 206

T-111

23,203 Grain Size 0.012 mm. 200X
DPH 265

ASTAR-811C

FIGURE 10 - Pre-Test Microstructure of Wrought-Recrystallized T-111 and ASTAR-811C.

23,225 Grain Size 0.031 mm. 100X
DPH 224

T-111

23,332 Grain Size 0.017 mm. 100X
DPH 286

ASTAR-811C

FIGURE 11 - Pre-Test Microstructure of T-111 and ASTAR-811C Sheet.

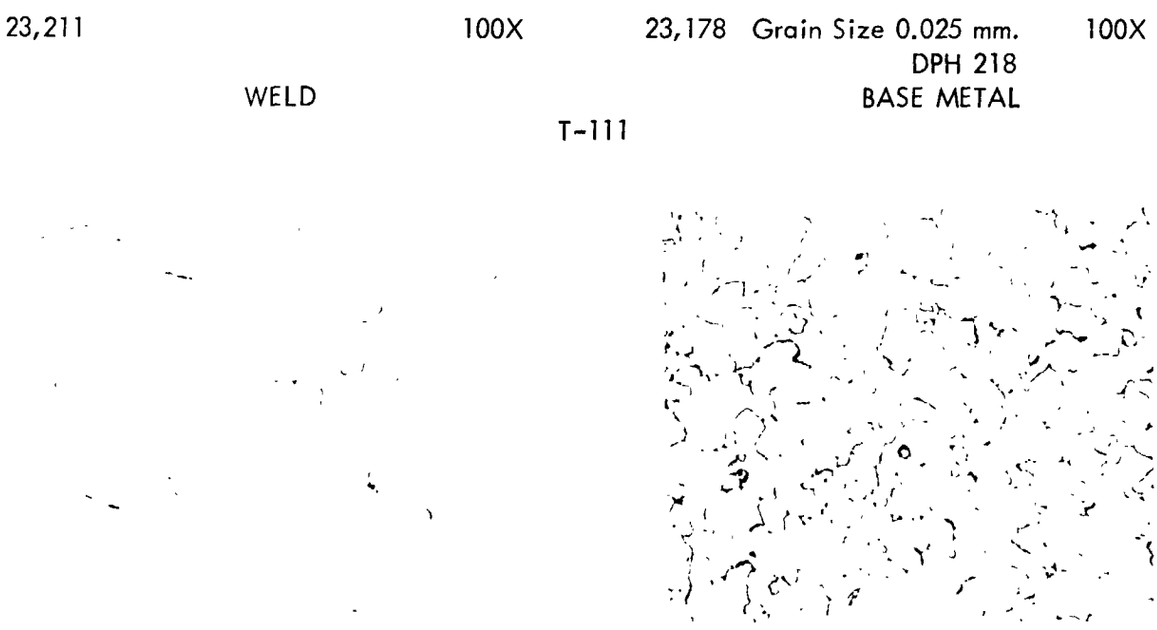

23,211 100X 23,178 Grain Size 0.025 mm. 100X
DPH 218
WELD BASE METAL

T-111

23,213 100X 23,214 Grain Size 0.026 mm. 100X
DPH 287
WELD/HAZ BASE METAL

ASTAR-811C

FIGURE 12 - Pre-Test Microstructure of the Weld Zone and Unaffected Base Metal in GTA Plate Welds in T-111 and ASTAR-811C.

T-111			Form	ASTAR-811C		
	Hardness[b]				Hardness[b]	
Gr. Size[a]	kg/mm^2	10^7 N/m^2		Gr. Size[a]	kg/mm^2	10^7 N/m^2
0.72 mm	190	186	As Cast[c]	0.8-1.2 mm	284	278
0.029	206	202	Wrt-Recryst.	0.012	265	260
0.031	224	220	Sheet	0.017	286	280
0.025	218	214	Plate Weld[d]	0.026	287	281

(a) Determined by linear intercept method.

(b) 10 kg (98.06 N) load.

(c) Average value - doesn't reflect orientation factors.

(d) For base metal only.

Test data are presented below by specimen type. Also provided are the results of visual and metallographic examinations of the individual specimens as well as the results of fractographic evaluations conducted with the scanning electron microscope (SEM).

As-Cast Specimens

Tensile tests were performed at five temperatures using three different strain rates at each temperature. Test temperatures were selected based on the results presented in Section 4.1 for the measurement of temperature time profiles in multipass GTA plate welds. Strain rates, selected to bracket the probable strain-time conditions pertinent to the deformation and grain boundary fracture behavior observed in plate welds, ranged from 0.005 $min.^{-1}$ to 2.0 $min.^{-1}$. Testing at a 0.005 $min.^{-1}$ strain rate is not generally sound engineering practice at pressures greater than 1.33×10^{-6} N/m^2 (10^{-8} torr) above 1649°C (3000°F), particularly for a carbide-strengthened alloy such as ASTAR-811C, due to the potential for decarburization. Hence, the minimum strain rate used for ASTAR-811C tests was 0.05 $min.^{-1}$, while several T-111 specimens were tested at 0.005 $min.^{-1}$.

The results of these tests are tabulated in Tables 8 and 9 for T-111 and ASTAR-811C, respectively. The effect of testing at the higher strain rates was to displace the tensile

TEST TEMPERATURES	TENSILE PROPERTY	TEST STRAIN RATE, min^{-1}			
		0.005	0.05	0.5	2.0
2200°F(1205°C)	UTS, ksi (10^7 N/m^2)	36.7 (25.3)	----	41.0 (28.3)	39.9 (27.5)
	0.2% Y.S., ksi (10^7 N/m^2)	28.3 (19.5)	----	27.1 (18.7)	25.4 (17.5)
	Unif. Elong., %	3.7	----	8.5	10.5
	Total Elong., %	6.4	----	12.0	14.8
2600°F(1427°C)	UTS, ksi (10^7 N/m^2)	----	24.6(17.0)	27.9 (19.2)	30.2 (20.8)
	0.2% Y.S., ksi(10^7 N/m^2)	----	22.5(15.5)	22.5 (15.5)	25.6 (17.6)
	Unif. Elong., %	----	1.1	2.5	2.2
	Total Elong., %	----	1.1	2.5	2.2
3000°F(1649°C)	UTS, ksi (10^7 N/m^2)	15.9 (11.0)	----	22.1 (15.2)	22.6 (15.6)
	0.2% Y.S., ksi (10^7 N/m^2)	----	----	21.5 (14.8)	21.0 (14.5)
	Unif. Elong., %	0.1	----	0.5	0.9
	Total Elong., %	0.1	----	1.0	1.3
3300°F(1816°C)	UTS, ksi (10^7 N/m^2)	8.1 (5.6)	----	16.5 (11.4)	19.6 (13.5)
	0.2% Y.S., ksi(10^7 N/m^2)	7.9 (5.4)	----	----	19.3 (13.3)
	Unif. Elong. , %	0.5	----	0.1	0.4
	Total Elong. , %	0.7	----	0.2	0.6
3600°F(1982°C)	UTS, ksi (10^7 N/m^2)	4.6 (3.2)	----	12.9 (8.9)	13.8 (9.5)
	0.2% Y.S., ksi (10^7 N/m^2)	4.4 (3.0)	----	12.7 (8.8)	13.8 (9.5)
	Unif. Elong., %	1.4	----	0.2	0.2
	Total Elong., %	3.9	----	0.3	0.4

TABLE 8 - Summary of Tensile Test Results on As-Cast T-111.
Test Temperatures and Strain Rates as Indicated.

		TENSILE PROPERTY	TEST STRAIN RATE, min^{-1}			
			0.005	0.05	0.5	2.0
TEST TEMPERATURES	2200°F(1205°C)	UTS, ksi (10^7 N/m^2)	----	61.1 (42.1)	62.0 (42.7)	62.6 (43.2)
		0.2%Y.S.,ksi (10^7 N/m^2)	----	41.7 (28.8)	41.3 (28.5)	38.5 (26.5)
		Unif. Elong.,%	----	6.7	8.8	14.5
		Total Elong.,%	----	11.8	15.0	21.6
	2600°F(1427°C)	UTS, ksi (10^7 N/m^2)	34.3 (23.6)	----	>40 (>27.6)[a]	41.8 (28.8)
		0.2%Y.S., ksi (10^7 N/m^2)	32.6 (22.5)	----	----	35.0 (24.1)
		Unif. Elong.,%	2.8	----	1.7[b]	7.2
		Total Elong.,%	14.4	----	----	12.1
	3000°F(1649°C)	UTS,ksi (10^7 N/m^2)	----	24.6 (17.0)	31.1 (21.4)	33.3 (23.0)
		0.2% Y.S., ksi(10^7 N/m^2)	----	24.6 (17.0)	30.8 (21.2)	----
		Unif. Elong.,%	----	0.2	0.5	0.2
		Total Elong.,%	----	1.0	0.6	0.3
	3300°F(1816°C)	UTS, ksi (10^7 N/m^2)	----	17.0 (11.7)	22.5 (15.5)	25.4 (17.5)
		0.2% Y.S., ksi (10^7 N/m^2)	----	15.5 (10.7)	21.0 (14.5)	23.0 (15.8)
		Unif. Elong.,%	----	1.3	4.1	3.3
		Total Elong.,%	----	4.2	5.3	4.0
	3600°F(1982°C)	UTS, ksi (10^7 N/m^2)	----	10.6 (7.3)	14.0 (9.6)	17.3 (11.9)
		0.2% Y.S.,ksi (10^7 N/m^2)	----	9.6 (6.6)	14.0 (9.6)	17.3 (11.9)
		Unif. Elong.,%	----	1.3	0.2	0.2
		Total Elong.,%	----	2.4	0.2	0.4

(a) - Specimen not fractured ; reached load limit of testing machine.
(b) - Measured elongation of the unfractured specimen.

TABLE 9 - Summary of Tensile Test Results on As-Cast ASTAR-811C. Test Temperatures and Strain Rates as Indicated.

property vs. test temperature data to slightly higher temperatures. Little effect of strain rate on fracture appearance was observed, the fracture appearance being predominantly a function of test temperature. Hence, primary emphasis of both the metallographic and fractographic evaluations was directed toward the specimens tested at the slower strain rates.

Comparison of the data for T-111 and ASTAR-811C confirms the expected greater high temperature strength of ASTAR-811C but indicates little difference in the ductility of the two alloys in the as-cast condition above 1427°C (2600°F).

The mechanical properties of these alloys are known to be influenced by the presence of hafnium as an alloying addition and, in the case of ASTAR-811C, the presence of intentionally added carbon. To assess the probable role of these factors on the observed ductility and fracture behavior of T-111 and ASTAR-811C, several tensile tests were performed on specimens of as-cast, EB melted Ta-10W alloy. The results of these tests are presented in Table 10, where the fracture strains are seen to be alarmingly low, much like those observed for T-111 and ASTAR-811C. This implies the very large grain size of the as-cast specimens may be largely responsible for the very low tensile elongations observed.

The coarse, planar appearance of the fracture surfaces of both alloys suggested grain boundary fracture. Typical examples of this are shown in Figure 13. Grain boundary delineation and cracking was observed along the gage lengths of the specimens tested at 1649°C (3000°F) and above, becoming most severe at 1982°C (3600°F), Figure 14. Ta-10W behaved in a manner identical to that of T-111 and ASTAR-811C, displaying severe gage length grain boundary cracking at 1649° and 1982°C (3000° and 3600°F). Specimens tested at 1205°C (2200°F), particularly ASTAR-811C and Ta-10W, failed in a chisel-point fracture approaching 100% reduction in area. Most of the specimens tested at the higher temperatures, despite the low total strain accommodation, exhibited regions of considerable localized deformation. This implies the observed behavior is not due to a true lack of ductility but rather due to the inability of the specimen to deform uniformly.

Test Temp.		UTS		0.2% Y.S.		% Elongation	
^{o}F	^{o}C	ksi	10^{7} N/m^{2}	ksi	10^{7} N/m^{2}	Unif.	Total
2200	1205	21.9	15.1	18.2	12.5	3.7	18.1
3000	1649	13.8	9.5	13.2	9.1	0.6	2.0
3600	1982	7.2	5.0	---	---	0.2	0.4

All tests at 0.005 min^{-1} strain rate throughout.

TABLE 10 - Tensile Test Results on As-Cast EB Melted Ta-10W Round Bar Specimens.

Tested at 3000°F (1649°C) 12X
at 0.005 min^{-1} strain rate

Tested at 3300°F (1816°C) 12X
at 0.005 min^{-1} strain rate

T-111

Tested at 3000°F (1649°C) 12X
at 0.05 min^{-1} strain rate.

ASTAR-811C

FIGURE 13 - Typical Fracture Surfaces of As-Cast T-111 and ASTAR-811C Specimens. Test Temperature and Strain Rate as Indicated.

Tested at 3600°F (1982°C) 12X
at 0.005 min^{-1} strain rate

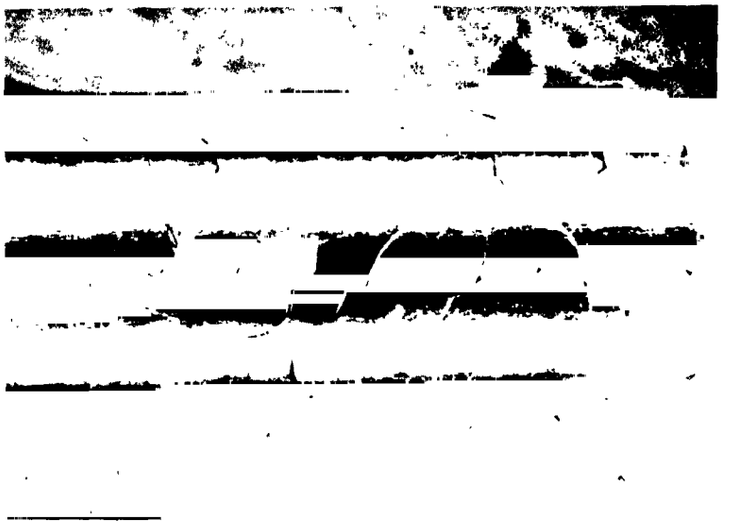

Tested at 3600°F (1982°C) at 0.005 min^{-1} strain rate 12X

FIGURE 14 - Fracture Surface and Gage Length of As-Cast T-111 Specimen Tested as Indicated.

Metallographic examination revealed the T-111 microstructures to be quite clean (i.e., free of general or localized precipitation). Internal grain boundaries, particularly those transverse to the stress axis, displayed evidence of void formation and intergranular cracking. Typical post-test microstructures of the as-cast T-111 are shown in Figure 15.

ASTAR-811C specimens demonstrated a lesser tendency toward internal grain boundary cracking than T-111 at most test temperatures. However, cracking was quite prominent in specimens tested at 1649°C (3000°F) and higher. Cracks were primarily along boundaries transverse to the stress axis (top, Figure 16) while boundaries oriented obliquely to the stress axis displayed the somewhat unusual appearance seen in the photomicrograph at the bottom of Figure 16. The region adjacent to the oblique boundary has apparently undergone extensive localized recrystallization, presumably as the direct result of the localized deformation occurring there during testing. Note the lack of deformation substructure in the areas away from the boundary.

SEM Fractography - The topology of the fracture surfaces was characterized by means of the scanning electron microscope (SEM). This comparatively new tool offers tremendous potential in the study of fractures due to its unique, invaluable large depth of field.

Scanning micrographs of the as-cast T-111 specimen tested at 1205°C (2200°F) are shown in Figure 17. Despite the "brittle" appearance at low magnifications, inspection at high magnifications reveals dimpled features characteristic of ductile fracture[9]. Note also the turbulent-appearing zone adjacent to the grain boundary in the 1000X micrograph. Dimpled rupture is shown in several different orientations in the T-111 specimen tested at 1427°C (2600°F), Figure 18. After testing at 1649°C (3000°F), where the fracture strain was only 0.1 percent, evidence of dimpled rupture persists, Figure 19. However, the size of the "zone" associated with the dimples appears to have increased.

Tested at 2600°F (1427°C) 1500X
at 0.05 min^{-1} strain rate
Fracture Strain 1.1%

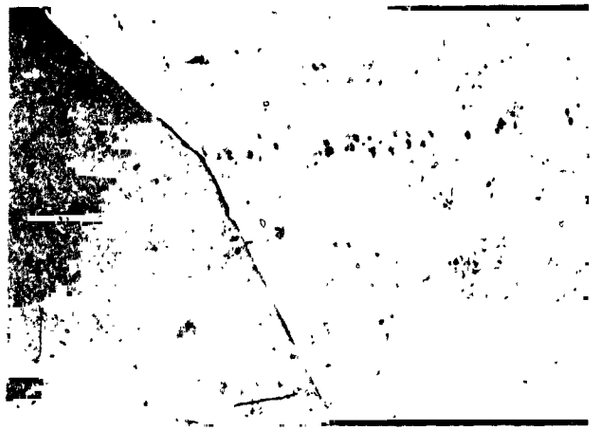

Tested at 3300°F (1816°C) 1500X
at 0.005 min^{-1} strain rate
Fracture Strain 0.7%

FIGURE 15 - Post-Test Microstructures of As-Cast T-111 Specimens. Test Conditions as Indicated.

Tested at 3300°F (1816°C)
at 0.05 min^{-1} strain rate

Stress Axis

Fracture Strain 4.2%

22,543 50X

Tested at 3000°F (1649°C)
at 0.05 min^{-1} strain rate

Stress Axis

Fracture Strain 1.0%

22,542 1500X

FIGURE 16 - Post - Test Microstructure of As-Cast ASTAR-811C Specimens. Test Conditions as Indicated.

Strain Rate 0.005 min^{-1}. Fracture Strain 6.4%.

FIGURE 17 - Scanning Electron Micrographs of the Fracture Surface of an As-Cast T-111 Specimen Tested at 2200°F (1205°C).

40X

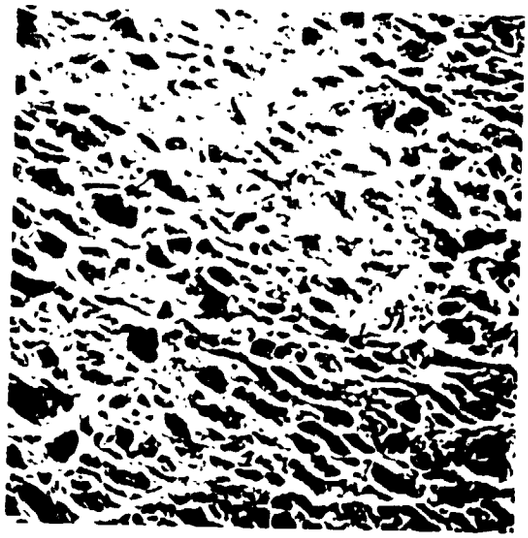

1000X

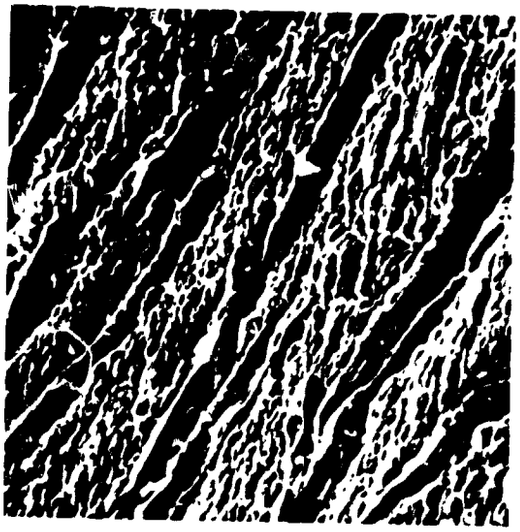

2000X

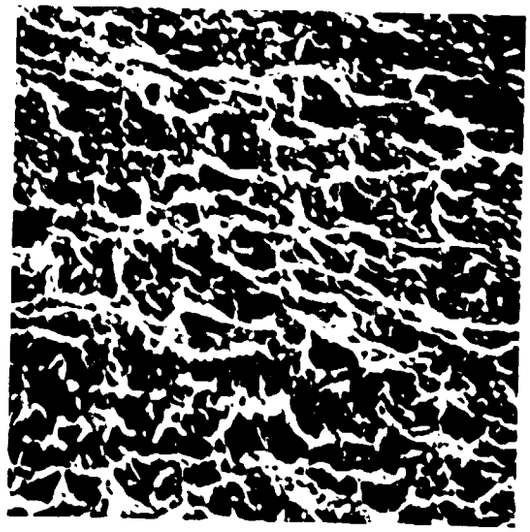

2000X

Strain Rate 0.05 min^{-1}. Fracture Strain 1.1%.

FIGURE 18 - Scanning Electron Micrographs of the Fracture Surface of an As-Cast T-111 Specimen Tested at 2600°F (1427°C).

50X

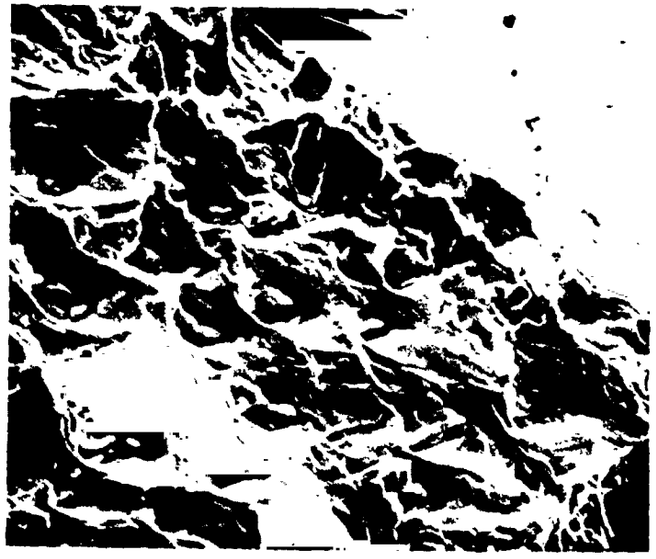

2000X

Strain Rate 0.005 min^{-1}. Fracture Strain 0.1%.

FIGURE 19 - Scanning Electron Micrographs of the Fracture Surface of an As-Cast T-111 Specimen Tested at 3000°F (1649°C).

The fracture surfaces of as-cast T-111 specimens tested at 1816° and 1982°C (3300° and 3600°F) exhibited general features much like those of the 1649°C (3000°F) specimen. Typical micrographs are shown in Figure 20 for the 1816°C (3300°F) test specimen. Figure 21 shows micrographs of another area on the fracture surface of the 1816°C (3300°F) specimen. The surface is marked with a high density of striations which, on inspection at higher magnifications, are seen to be associated with microvoids (~0.5 μm. in diameter) at their apparent point of initiation. Very small precipitates are associated with several of the microvoids. Attempts to identify these with the x-ray spectrometer attachment to the SEM were unsuccessful due to their very small size. The unusual appearance of this surface is believed to be due to the unique conditions under which this grain boundary region deformed during testing. Correlation of the micrographs with the macroscopic fracture surface revealed this grain boundary region was disposed to the axis of the applied stress in such a way as to subject it to a stress system having a very high shear component. From the appearance of the striations we can infer at least two, and possibly more, separate shearing motions occurred. The change in direction of the striations implies that as the total system (i.e., this grain and at least the immediately adjoining grains) deformed the relative motion of the two grains forming the interface shown in Figure 21 occurred in two directions, apparently in alternating fashion.

Representative micrographs of the fracture surfaces of the as-cast ASTAR-811C specimens tested at 1427°, 1649° and 1816°C (2600°, 3000° and 3300°F) are shown in Figures 22 and 23. Differences between the two alloys are not large although, except for the 1649°C (3000°F) test, the ductility loss is not quite as drastic in ASTAR-811C.

Wrought-Recrystallized Specimens

Tensile tests were performed on T-111 and ASTAR-811C specimens at 1427°, 1649° and 1816°C (2600°, 3000° and 3300°F) using a constant 0.05 $min.^{-1}$ strain rate throughout all tests. Test results are presented for both alloys in Table II. Comparison with the data for as-cast material, Tables 8 and 9, reveals a tremendous increase in total tensile elongation for the wrought-recrystallized specimens whereas the other tensile properties are quite similar.

40X

200X

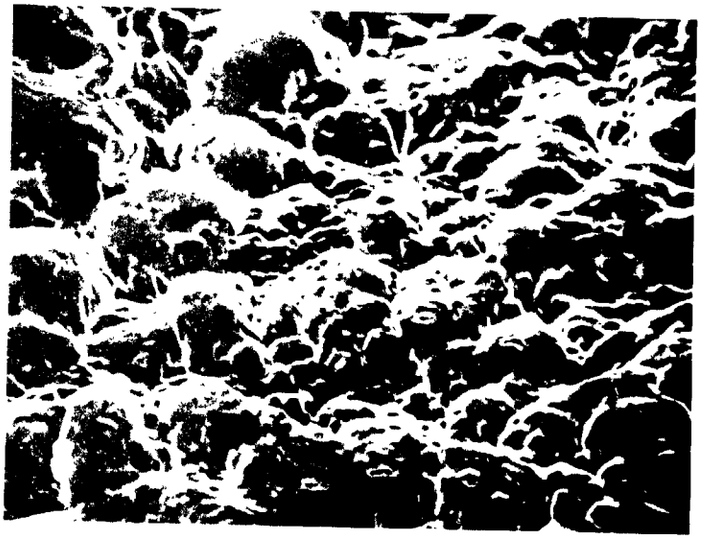

1000X

Strain Rate 0.005 min^{-1}. Fracture Strain 0.7%.

FIGURE 20 - Scanning Electron Micrographs of the Fracture Surface of an As-Cust T-111 Specimen Tested at 3300°F (1816°C).

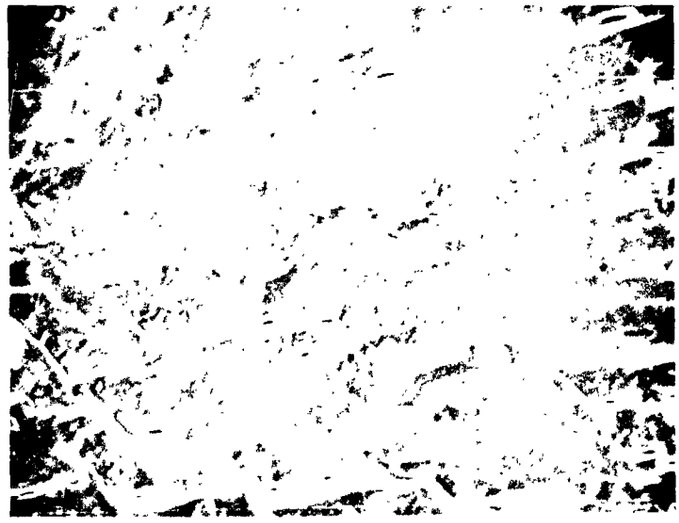

1000X

4000X

Strain Rate 0.005 min^{-1}. Fracture Strain 0.7%.

FIGURE 21 - Scanning Electron Micrographs of the Fracture Surface of an As-Cast T-111 Specimen Tested at 3300°F (1816°C).

40X

1800X

7200X

Strain Rate 0.005 min^{-1}.

Fracture Strain 14.4%.

FIGURE 22 - Scanning Electron Micrographs of the Fracture Surface of an As-Cast ASTAR-811C Specimen Tested at 2600°F (1427°C).

40X

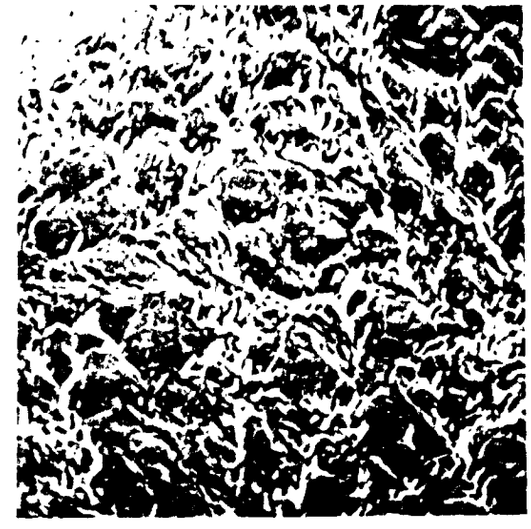

1000X

Strain Rate 0.05 min^{-1}. Fracture Strain 1.0%.
Tested at 3000°F (1649°C)

40X

Strain Rate 0.05 min^{-1}. Fracture Strain 4.2%.
Tested at 3300°F (1816°C)

FIGURE 23 - Scanning Electron Micrographs of the Fracture Surface of As-Cast ASTAR-811C Specimens Tested as Indicated.

Alloy	Test Temp.		UTS		0.2% Y.S.		% Elongation	
	^{o}F	^{o}C	ksi	10^7 N/m^2	ksi	10^7 N/m^2	Unif.	Total
T-111	2600	1427	31.3	21.6	24.1	16.6	11.0	31.0
T-111	3000	1649	20.3	14.0	20.2	13.9	1.5	46.1
T-111	3300	1816	12.6	8.7	11.5	7.9	0.4	71.6
ASTAR-811C	2600	1427	39.9	27.5	36.0	24.8	1.2+	(a)
ASTAR-811C	3000	1649	23.4	16.1	23.2	16.0	0.5	71.9
ASTAR-811C	3300	1816	16.3	11.2	16.3	11.2	0.6	64.2

(a) No fracture ; reached load limit of testing machine.

0.05 min^{-1} strain rate used throughout all tests.

TABLE 11 - Summary of Tensile Test Results on Wrought-Recrystallized T-111 and ASTAR-811C.

The extremely fine grain size of these materials made it impossible to view the fracture surfaces directly with the optical microscope. Pesults of metallographic examination of the T-111 specimens are presented in Figures 24 through 26. At 1427°C (2600°F), Figure 24, the cracking is entirely intergranular and is most severe on transverse boundaries. At high magnifications the serrated, irregular character of the grain boundary regions is apparent. After testing at 1649°C (3000°F), Figure 25, the grain boundary distortion and serration is greater and more evidence of intragranular deformation is seen. Despite the high fracture strain at 1816°C (3300°F) the intergranular cracking is extremely severe, Figure 26. The irregularly shaped grain boundaries seen in the 1500X photos hcve undergone considerable change in position under the combined influence of high test temperature and applied stress.

The 1427°C (2600°F) ASTAR-811C specimen was not fractured due to the load limit of the testing machine being used. Only about 1% plastic strain was achieved and, as reference to Figure 27 shows, the microstructure was unaffected. Testing ASTAR-811C at 1649°C (3000°F), Figure 28, resulted in much less intergranular cracking than was observed for similar tests on T-111 (Figure 25). The regions adjacent to the grain boundaries have undergone considerable local change, including grain boundary migration and substructure development. The specimen tested at 1816°C (3300°F), Figure 29, looked quite similar to the 1649°C (3000°F) specimen except possibly that a small amount of grain growth had occurred at the higher test temperature.

SEM Fractography - Only the specimens tested at 1649° and 1816°C (3000° and 3300°F) were examined with the scanning electron microscope. Typical micrographs of the fracture surface are shown in Figure 30. Despite the widespread intergranular cracking which occurs during deformation the fracture appears to have occurred by ductile rupture of the individual grains comprising the fracture surface.

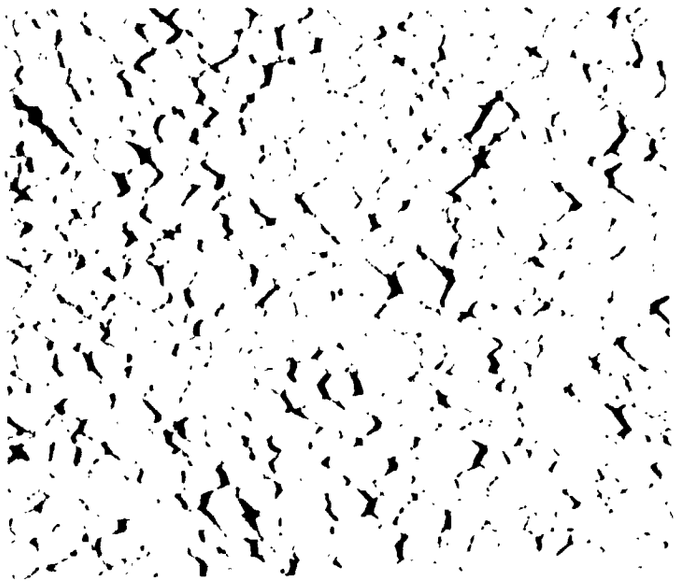

100X

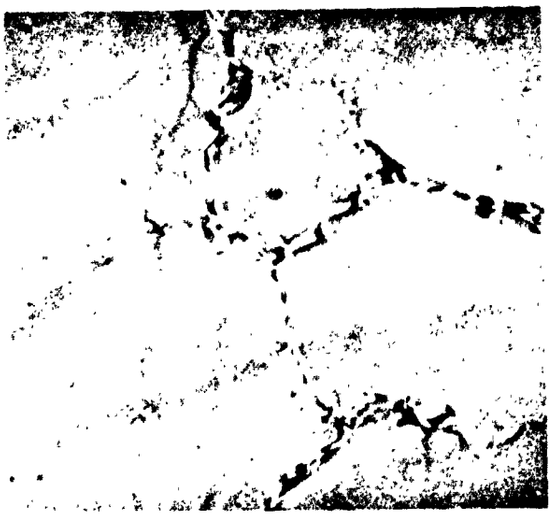

1500X

1500X

23,171

Strain Rate 0.05 min^{-1}. Fracture Strain 31.0%.

FIGURE 24 - Post-Test Microstructure of Wrought-Recrystallized T-111 Specimen Tested at 2600°F (1427°C).

100X

750X

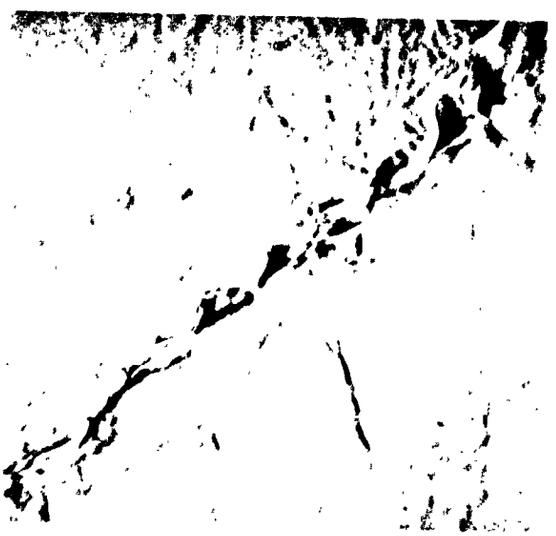

1500X

23,205

Strain Rate 0.05 min^{-1}. Fracture Strain 46.1%.

FIGURE 25 - Post-Test Microstructure of Wrought-Recrystallized T-111 Specimen Tested at 3000°F (1649°C).

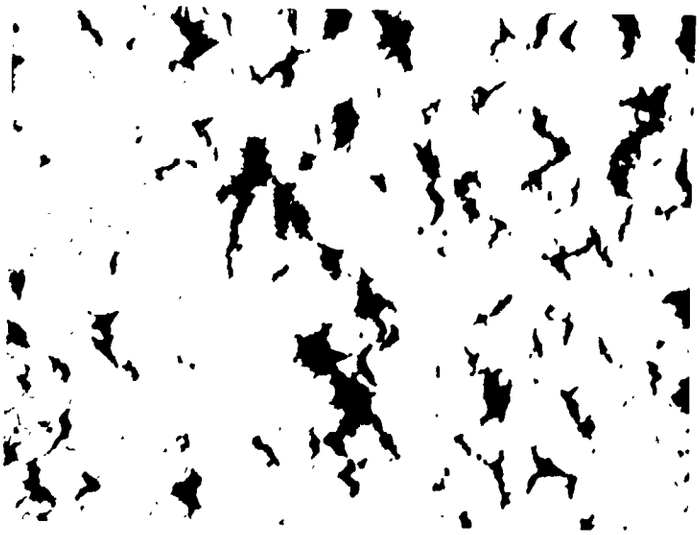

100X

1500X

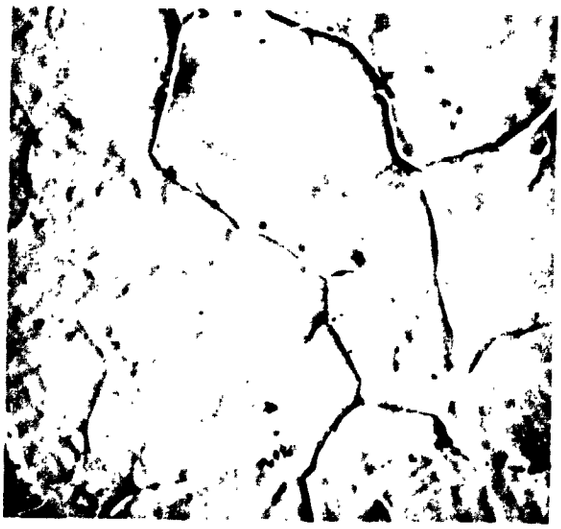

1500X

23,172

Strain Rate 0.05 min^{-1}. Fracture Strain 71.6%.

FIGURE 26 - Post-Test Microstructure of Wrought-Recrystallized T-111 Specimen Tested at 3300°F (1816°C).

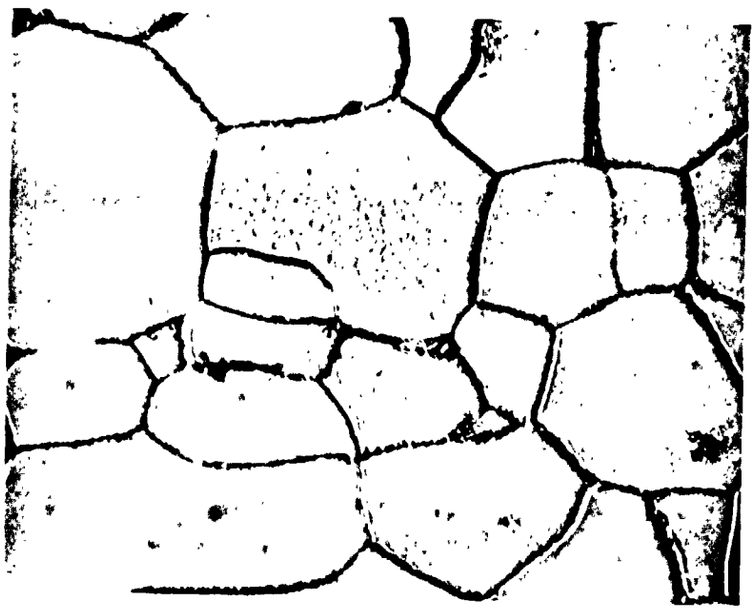

23,203 1500X

Strain Rate 0.05 min^{-1}. Specimen not fractured.

FIGURE 27 - Post-Test Microstructure of Wrought-Recrystallized ASTAR-811C Specimen Tested at 2600°F (1427°C).

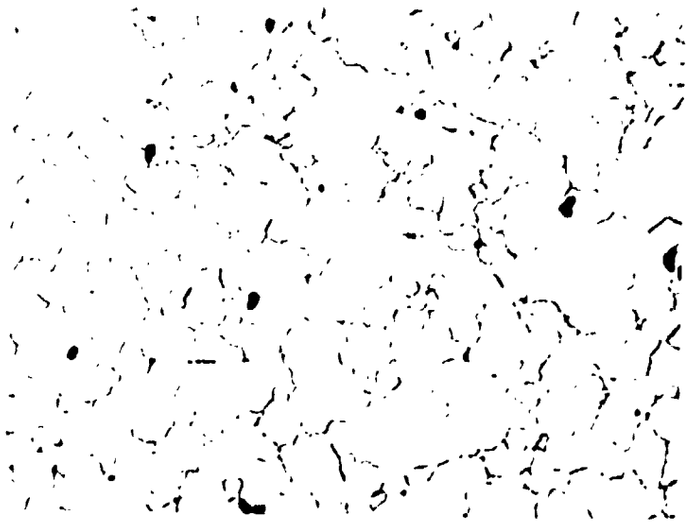

400X

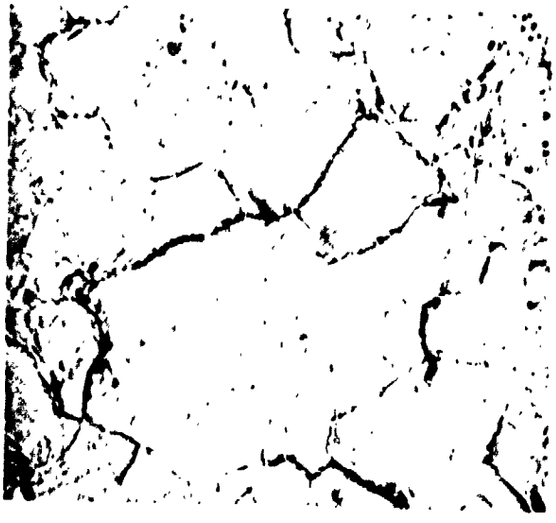

1500X

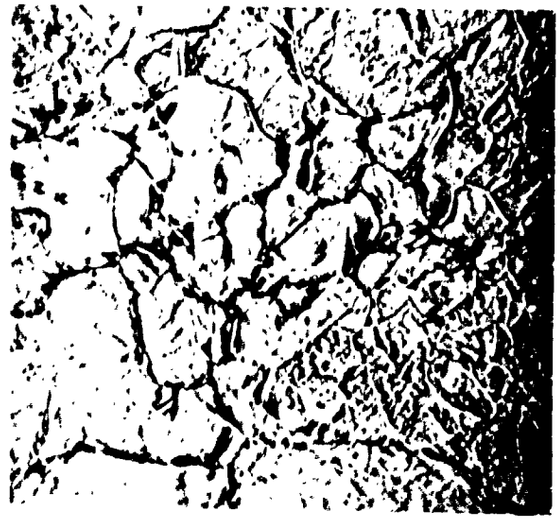

1500X

23,175

Strain Rate 0.05 min^{-1}. Fracture Strain 71.9%.

FIGURE 28 - Post-Test Microstructure of Wrought-Recrystallized ASTAR-811C Specimen Tested at 3000°F (1649°C).

1500X

1500X

1500X

23,204

Strain Rate 0.05 min^{-1}. Fracture Strain 64.2%.

FIGURE 29 - Post-Test Microstructure of Wrought-Recrystallized ASTAR-811C Specimen Tested at 3300°F (1816°C).

200X

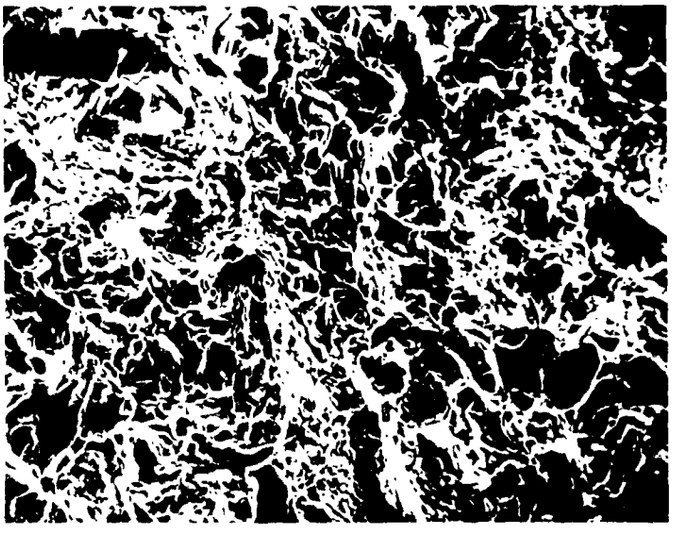

1000X

Strain Rate 0.05 min^{-1}. Fracture Strain 71.9%.

FIGURE 30 - Scanning Electron Micrographs of the Fracture Surface of a Wrought-Recrystallized ASTAR-811C Specimen Tested at 3000°F (1649°C).

GTA Sheet Weld Specimens

Tensile tests were performed on single pass GTA sheet weld specimens in T-111 and ASTAR-811C in two separate evaluations. The first set of tests were performed to duplicate the test conditions used for the wrought-recrystallized material reported in the preceding section. The results of these tests are presented in tabular form in Table 12. All tests were run using a constant 0.05 $min.^{-1}$ strain rate throughout.

In addition, tensile tests were performed at 982°, 1205°, 1427°, 1538°, 1760° and 1982°C (1800°, 2200°, 2600°, 2800°, 3200° and 3600°F) on a series of T-111 and ASTAR-811C longitudinal GTA-welded specimens. The initial intent of these tests was to permit evaluation of the possible role of grain boundary sliding in tensile deformation at moderate strain rates. Hence, prior to testing, the gage lengths of these specimens were metallographically polished and scribed with grid lines. All tests were performed using a constant 0.005 $min.^{-1}$ strain rate throughout. Results of these tests are presented in Table 13. Apparent differences in the property data of Tables 12 and 13 are largely due to the higher strain rate used to generate the test data of Table 12.

The relative contribution of grain boundary sliding to total strain is known to increase with decreasing strain rate and increasing test temperature. Post-test examination of the tensile specimens which were grid-lined prior to testing indicated that at the strain rate - test temperature conditions employed the contribution of grain boundary sliding to total strain was quite small. The fine grain structure of the weld specimens further complicates the analysis by making available a large number of grain boundaries to accommodate the total sliding strain. Hence, the sliding strain observed at any given boundary is extremely small.

The data of both Tables 12 and 13 indicate greater ductility for the ASTAR-811C specimens than for the T-111 specimens. This is consistent with the general trend observed for the other types of specimens reported previously. The results of optical metallographic examinations of the specimens represented on Tables 12 and 13 are summarized below:

Alloy	Test Temp.		UTS		0.2% Y.S.		% Elongation	
	°F	°C	ksi	10^7 N/m^2	ksi	10^7 N/m^2	Unif.	Total
T-111	2600	1427	29.3	20.2	25.7	17.7	1.6	3.1
T-111	3000	1649	18.6	12.8	17.5	12.1	1.7	3.5
T-111	3300	1816	12.6	8.7	11.5	7.9	5.1	10.4
ASTAR-811C	2600	1427	47.9	33.0	35.9	24.8	5.0	16.7
ASTAR-811C	3000	1649	24.1	16.6	22.2	15.3	3.7	18.2
ASTAR-811C	3300	1816	15.8	10.9	10.8	7.4	18.9	46.5

0.05 min^{-1} strain rate used throughout all tests.

TABLE 12 - Summary of Tensile Test Results on Longitudinal GTA Sheet Weld Specimens in T-111 and ASTAR-811C Sheet.

Alloy	Test Temp.		UTS		0.2% Y.S.		% Elongation	
	°F	°C	ksi	10^7 N/m^2	ksi	10^7 N/m^2	Unif.	Total
T-111	1800	982	58.6	40.4	39.0	26.9	8.9	14.6
T-111	2200	1205	37.3	25.7	22.4	15.4	3.1	7.6
T-111	2600	1427	23.3	16.1	20.5	14.1	1.4	4.8
T-111	2800	1538	17.8	12.3	16.8	11.6	1.2	4.8
T-111	3200	1760	7.2	5.0	5.5	3.8	11.2	27.0
T-111	3600	1982	4.1	2.8	2.4	1.6	10.2	72.8
ASTAR-811C	1800	982	>77.5	>53.4	50.6	34.9	6.0	>19.0[(a)]
ASTAR-811C	2200	1205	65.5	45.2	46.8	32.3	7.0	20.6
ASTAR-811C	2600	1427	40.3	27.8	36.2	25.0	3.2	14.8
ASTAR-811C	2800	1538	29.6	20.4	26.2	18.1	1.5	9.8
ASTAR-811C	3200	1760	10.2	7.0	7.5	5.2	9.7	40.5
ASTAR-811C	3600	1982	4.2	2.9	1.6	1.1	22.4	49.1

0.005 min^{-1} strain rate used throughout all tests.

(a) No fracture ; reached load limit of testing machine.

TABLE 13 - Summary of Tensile Test Results on Longitudinal GTA Sheet Weld Specimens in T-111 and ASTAR-811C Sheet. Used for Grain Boundary Sliding Study.

- Fractures of specimens tested at 982°C (1800°F) to about 1427°C (2600°F) appeared to have largely been the result of transgranular shear.
- At 1427°C (2600°F) and higher, although shear retained a prominent role in the deformation and fracture process, a greater percentage of the fracture surface was grain boundary in appearance.
- At 982°C (1800°F) and 1205°C (2200°F) intergranular cracking in the gage length was mainly confined to the regions near the fractured surface.
- As the test temperature increased the intergranular cracking in the gage length became more severe and was no longer confined to the regions near the fracture. At 1760°C (3200°F) particularly, the grain boundary cracking was catastrophic throughout the gage length.

Differences in fracture appearance and severity of intergranular cracking as a function of test temperature are shown for two typical T-111 specimens in Figure 31. The shear-type fracture behavior of ASTAR-811C at the lower test temperatures, Figure 32, is seen to be similar to that of T-111.

SEM Fractography - Scanning micrographs of the ASTAR-811C specimen tested at 1538°C (2800°F) are shown in Figure 33. This specimen failed after 9.8% strain and despite the apparent grain boundary nature of the fracture at 40X, many regions of the fracture surface at high magnifications, such as the 2000X micrograph shown, exhibit ductile, dimpled rupture characteristics.

Plate Weld Specimens

The final phase of tensile testing was directed toward evaluating the effectiveness of very high temperature homogenization annealing in alleviating the propensity for low strain, intergranular failures. Manual, multipass GTA plate welds were prepared using 0.952 cm (3/8 inch) thick T-111 and ASTAR-811C. Tensile specimens were machined from these welds in such a way that the axis of the weldment was transverse to the specimen's tensile axis. Identical specimens of each alloy were tested at 1649°C (3000°F) in the as-welded condition and after a 1 hour - 2483°C (4500°F) homogenization anneal. Decarburization

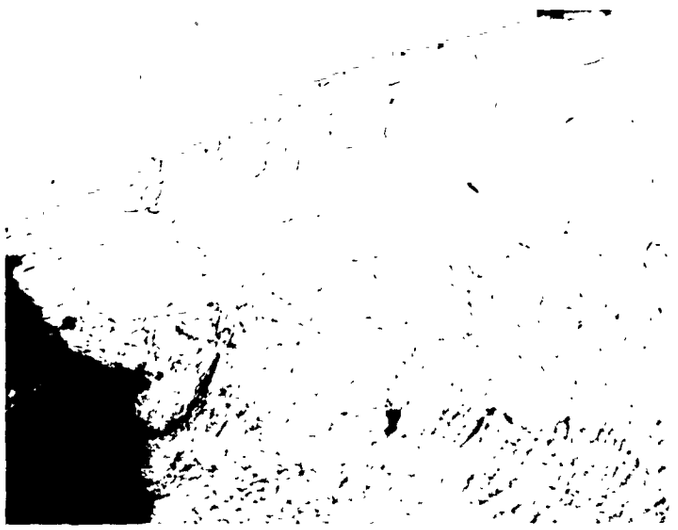

HAZ

Strain Rate 0.005 min^{-1}.

Fracture Strain 14.6%.

Tested at 1800°F (982°C).

Weld

23,225 100X

Stress Axis

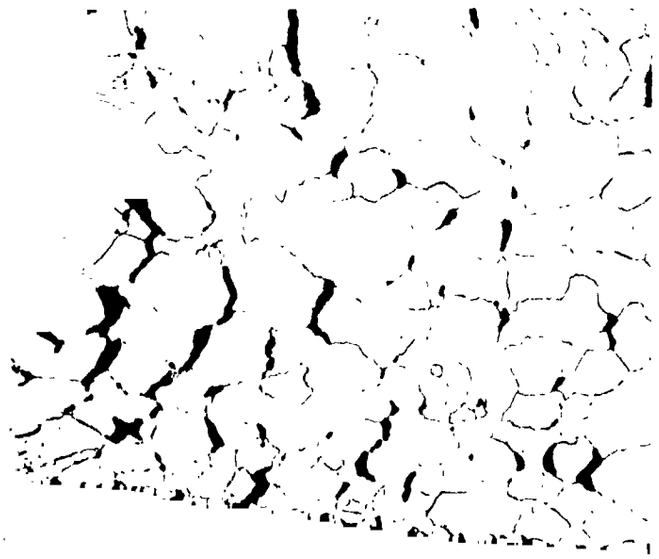

Weld

Strain Rate 0.005 min^{-1}.

Fracture Strain 27.0%.

Tested at 3200°F (1760°C).

HAZ

23,229 100X

FIGURE 31 - Post-Test Microstructure of T-111 GTA Weld Specimens Tested as Indicated.

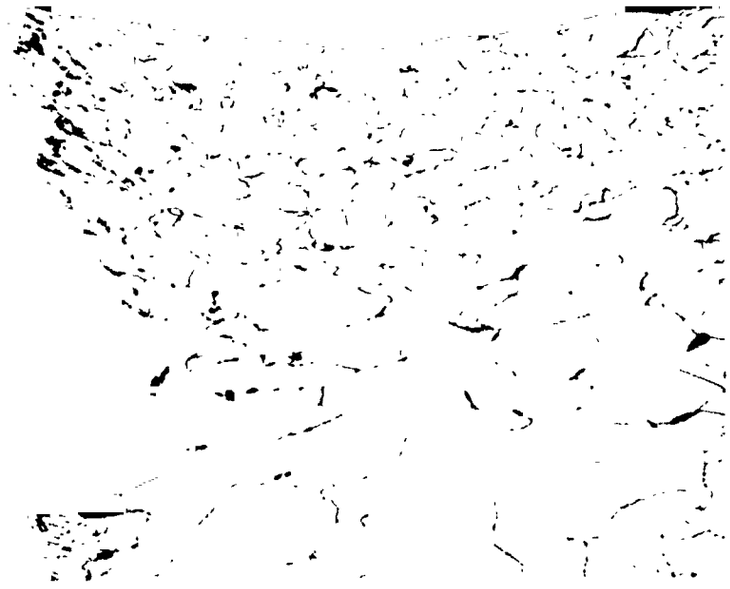

Strain Rate 0.005 min^{-1}. Fracture Strain 20.6 %.

Stress Axis

FIGURE 32 - Post-Test Microstructure of ASTAR-811C GTA Weld Specimen Tested at 2200°F (1205°C).

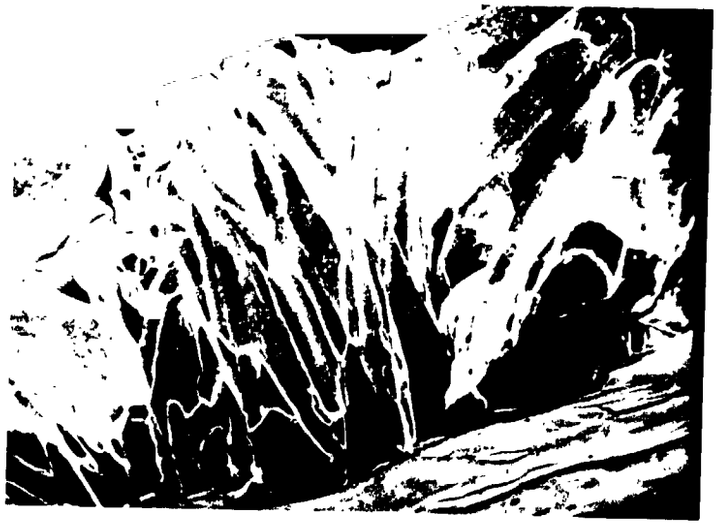

40X

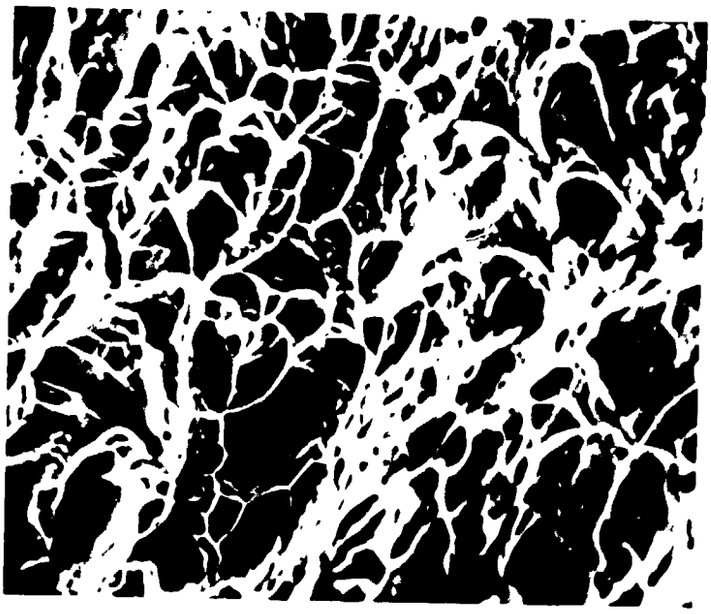

2000X

Strain Rate 0.005 min^{-1}. Fracture Strain 9.8%.

FIGURE 33 - Scanning Electron Micrographs of the Fracture Surface of an ASTAR-811C GTA Weld Specimen Tested at 2800°F (1538°C).

during annealing was prevented by encasing the specimens in a vacuum tight ASTAR-811C "envelope" which was welded shut after insertion of the specimens.

The results of these tests are presented in Table 14. The extremely low fracture strain values of the 2483°C (4500°F) annealed specimens appear to be the direct result of the very large grain size produced. In that respect, the effect of annealing at 2483°C (4500°F) had a negative result, promoting rather than preventing fracture at low total strain.

The results of post-test metallography on the as-welded T-111 specimen tested at 1649°C (3000°F) is shown in Figure 34. The fracture mode is intergranular, occurring mainly in the fusion zone. Except for grain boundary underbead cracking, shown in the bottom of Figure 34 to be present prior to testing, there is little evidence of general intergranular cracking prior to failure. After the 2483°C (4500°F) anneal, one or two grains occupied the entire cross section of the specimen. This is shown by the scanning electron microscopy below.

SEM Fractography - The fracture surfaces of the as-welded T-111 and ASTAR-811C specimens after testing at 1649°C (3000°F) are shown in Figures 35 and 36, respectively. The grain boundary character of the fractures is apparent. Note also at higher magnifications the areas of localized ductile rupture, particularly for ASTAR-811C, Figure 36.

Scanning micrographs of the T-111 specimen annealed at high temperature prior to testing are presented in Figure 37. Despite the planar appearance of the fracture at low magnifications, higher magnifications reveal areas which have "dimpled" rupture charccteristics. In this respect, these specimens are very much like the previously discussed coarse-grained as-cast specimens. The high temperature annealed ASTAR-811C specimen, not shown, displayed identical general features.

Alloy	Pre-Test History	UTS		0.2% Y.S.		% Elongation	
		ksi	10^7 N/m^2	ksi	10^7 N/m^2	Unif.	Total
T-111	As-Welded	19.0	13.1	18.6	12.8	1.7	2.4
T-111	1 hr.-4500°F (2483°C)	21.3	14.7	21.3	14.7	0.2	0.4
ASTAR-811C	As-Welded	23.1	15.9	22.3	15.4	2.5	6.2
ASTAR-811C	1 hr.-4500°F (2483°C)	22.3	15.4	22.3	15.4	0.1	0.4

0.05 min^{-1} strain rate used throughout all tests.

All tests performed at 3000°F.

TABLE 14 - Summary of Tensile Test Results on T-111 and ASTAR-811C Specimens Machined from 0.375 inch (0.952 cm.) Plate Welds.

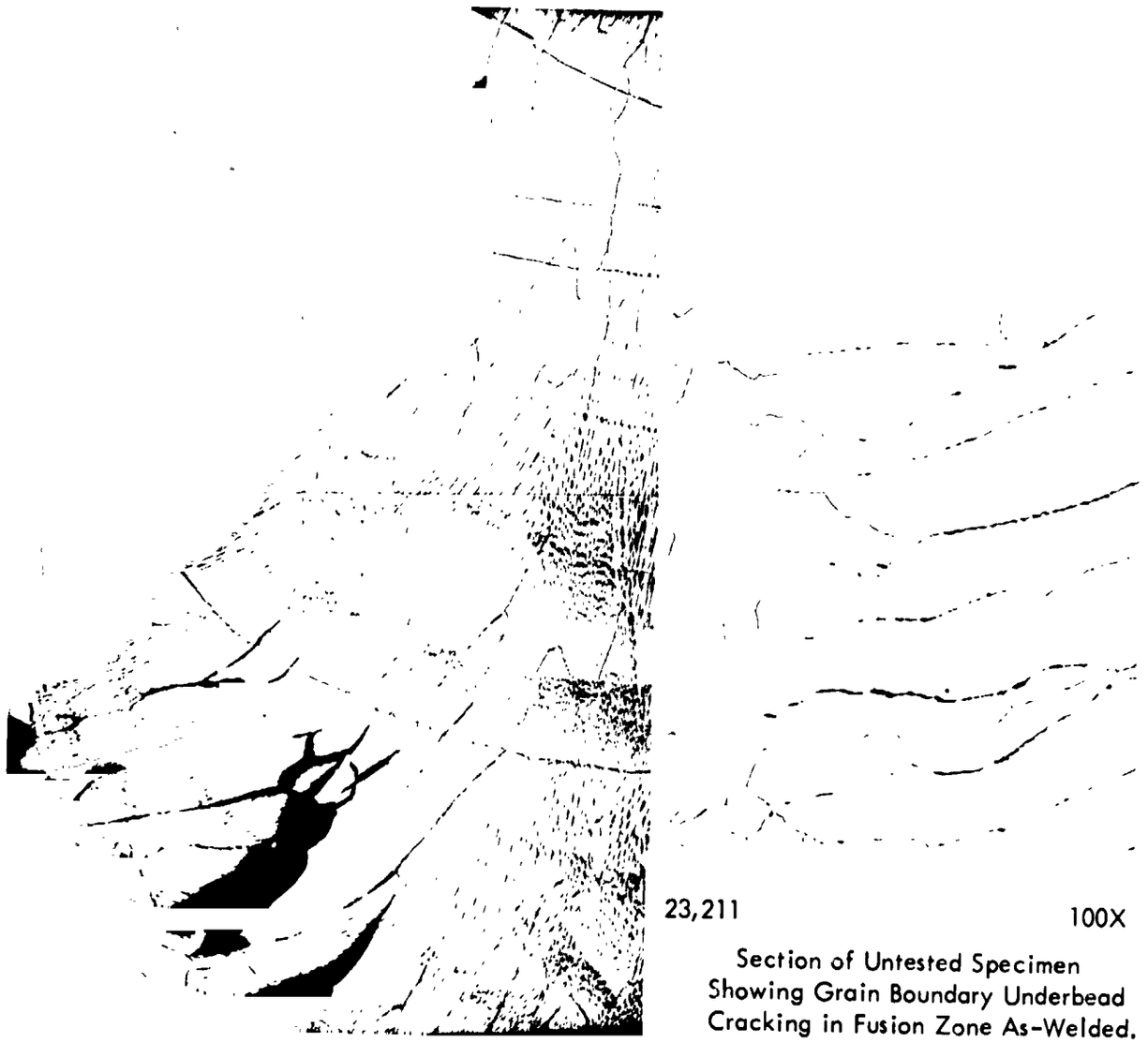

23,178

50X

Strain Rate 0.05 min^{-1}. Fracture Strain 2.4%.

23,211

100X

Section of Untested Specimen Showing Grain Boundary Underbead Cracking in Fusion Zone As-Welded.

FIGURE 34 - Microstructure of T-111 Tensile Specimens Machined from Multipass GTA Plate Weld. Tested at 3000°F (1649°C).

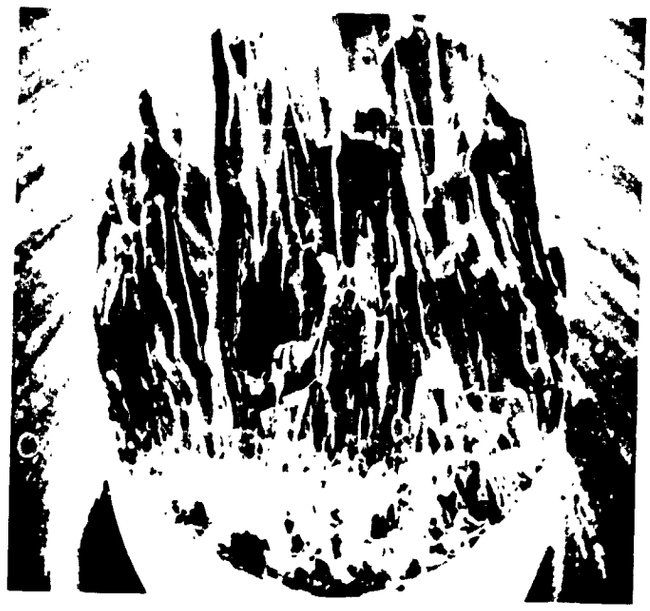

24X

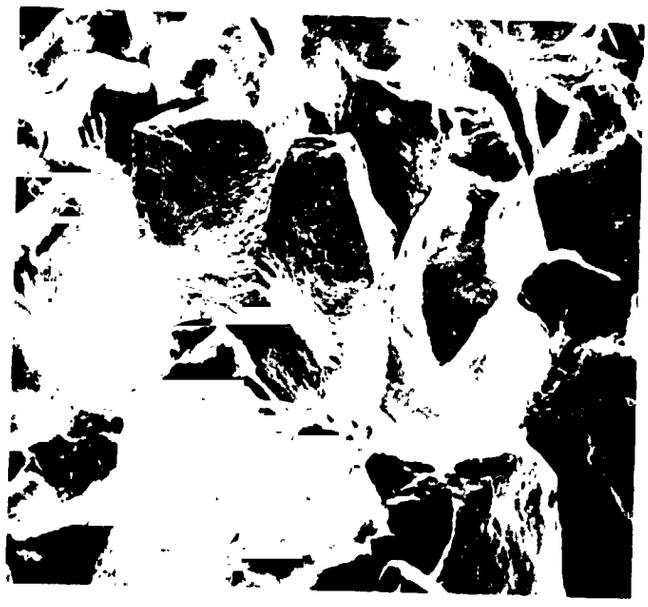

240X

Strain Rate 0.05 min^{-1}. Fracture Strain 2.4%.

FIGURE 35 - Scanning Electron Micrographs of the Fracture Surface of a T-111 Specimen Machined from a Multipass GTA Plate Weld. Tested in the As-Welded Condition at 3000°F (1649°C).

24X

240X

Strain Rate 0.05 min^{-1}. Fracture Strain 6.2%.

FIGURE 36 - Scanning Electron Micrographs of the Fracture Surface of an ASTAR-811C Specimen Machined from a Multipass GTA Plate Weld. Tested in the As-Welded Condition at 3000°F (1649°C).

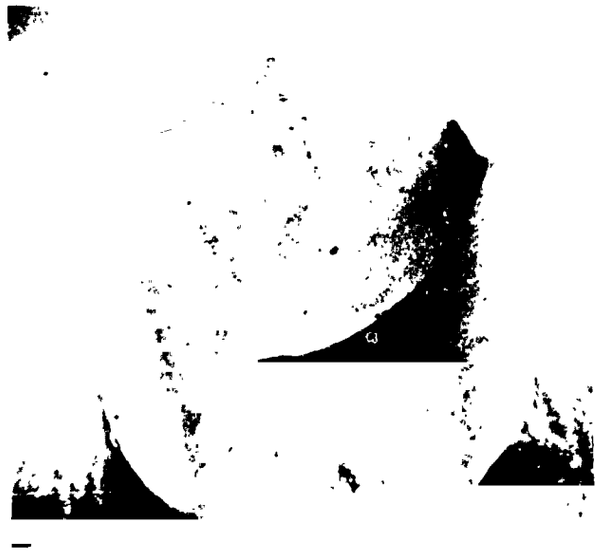

24X

600X

2400X

Strain Rate 0.05 min^{-1}. Fracture Strain 0.4%.

FIGURE 37 - Scanning Electron Micrographs of the Fracture Surface of a T-111 Specimen Machined from a Multipass GTA Plate Weld. Annealed 1 hour at 4500°F (2483°C) Prior to Testing.

4.3 Creep Testing

A series of T-111 and ASTAR-811C single pass longitudinal GTA welded sheet specimens were creep tested at temperatures ranging from 1316° through 1538°C (2400° through 2800°F). All tests were conducted in ultra-high vacuum, with pressures maintained $<1.33\times10^{-6}$ N/m^2 ($<10^{-8}$ torr) throughout. A summary of the test data is provided in Table 15. Except for 1 ASTAR-811C specimen, which was tested in the as-welded condition, all specimens were annealed 4 hours at 1982°C (3600°F) prior to testing. This was done in an effort to obtain a larger, more equi-axed grain structure. Adjustments in test conditions during testing indicated in Table 15 were made so that the 5000 hours total test time stipulated by the contract could be accumulated with the limited number of specimens available. The hardness of the T-111 specimens decreased slightly during testing. A more significant hardness decrease was observed for the ASTAR-811C specimens tested at 1316°C (2400°F). This likely reflects an aging reaction which is effecting the removal of carbon from solid solution. Conversely to this behavior, the hardness of the ASTAR-811C specimen tested at 1427°/1538°C (2600°/2800°F) increased slightly. This is due to the greater solubility of carbon at the higher temperature, hence as the temperature was raised to 1538°C (2800°F) precipitate dissolution occurred and the matrix hardness increased.

Individual creep curves are presented in Figures 38 through 43. Due to the complexity and changing conditions of the creep testing no attempt was made to analyze the data in terms of the stress or temperature dependence of creep. Any attempt to do so on data of such a limited nature was felt to be naive and unjustified. Parametric analysis, by means of the Larson-Miller parameter, indicated both the T-111 and ASTAR-811C data to be consistent with previously published work[10]. The results of this analysis are presented in Table 16. Only segments of the creep curves which displayed a reasonable amount of steady-state creep were included in the analysis.

Fractures were mainly grain boundary in character although in several cases transgranular shear did play a significant role. Representative areas are shown in Figure 44. Intergranular

Alloy	Spec. No.	Test Temp.		Stress		Time	Rupture	10 Kg(98.06N) Hardness			
								Start		Finish	
		°F	°C	ksi	10^7 N/m^2	hrs.	Strain(%)[a]	Kg/mm^2	10^7 N/m^2	Kg/mm^2	10^7 N/m^2
T-111	1	2400	1316	18.0	12.41	1.0					
		"	"	15.0	10.34	66.5	2.49	210	206	203	199
T-111	2	2400	1316	7.0	4.83	306.8					
		"	"	8.5	5.86	312.4					
		"	"	10.0	6.90	211.6					
		"	"	11.5	7.93	342.3	3.63	214	210	209	205
T-111	3	2600	1427	6.0	4.14	977.7	12.25	206	202	208	204
ASTAR-811C	1[b,c]	2400	1316	18.0	12.41	161.9					
		"	"	22.0	15.17	271.9	11.37	322	316	253	248
ASTAR-811C	2[c]	2400	1316	18.0	12.41	955.8					
		"	"	"	"	500.7	4.02	284	278	250	245
ASTAR-811C	3	2600	1427	7.0	4.83	452.5					
		2800	1538	"	"	386.5	5.47	283	277	309	303

(a) Determined after cooling to room temperature.
(b) Specimen tested as-welded. All others annealed 4 hrs-3600°F (1982°C) prior to testing.
(c) Test stopped, specimen examined and reloaded for further testing.
(d) Elongation after a total of 1456.5 hours - specimen not fractured.

TABLE 15 - Summary of Creep Test Data for T-111 and ASTAR-811C Longitudinal GTA Sheet Weld Specimens.

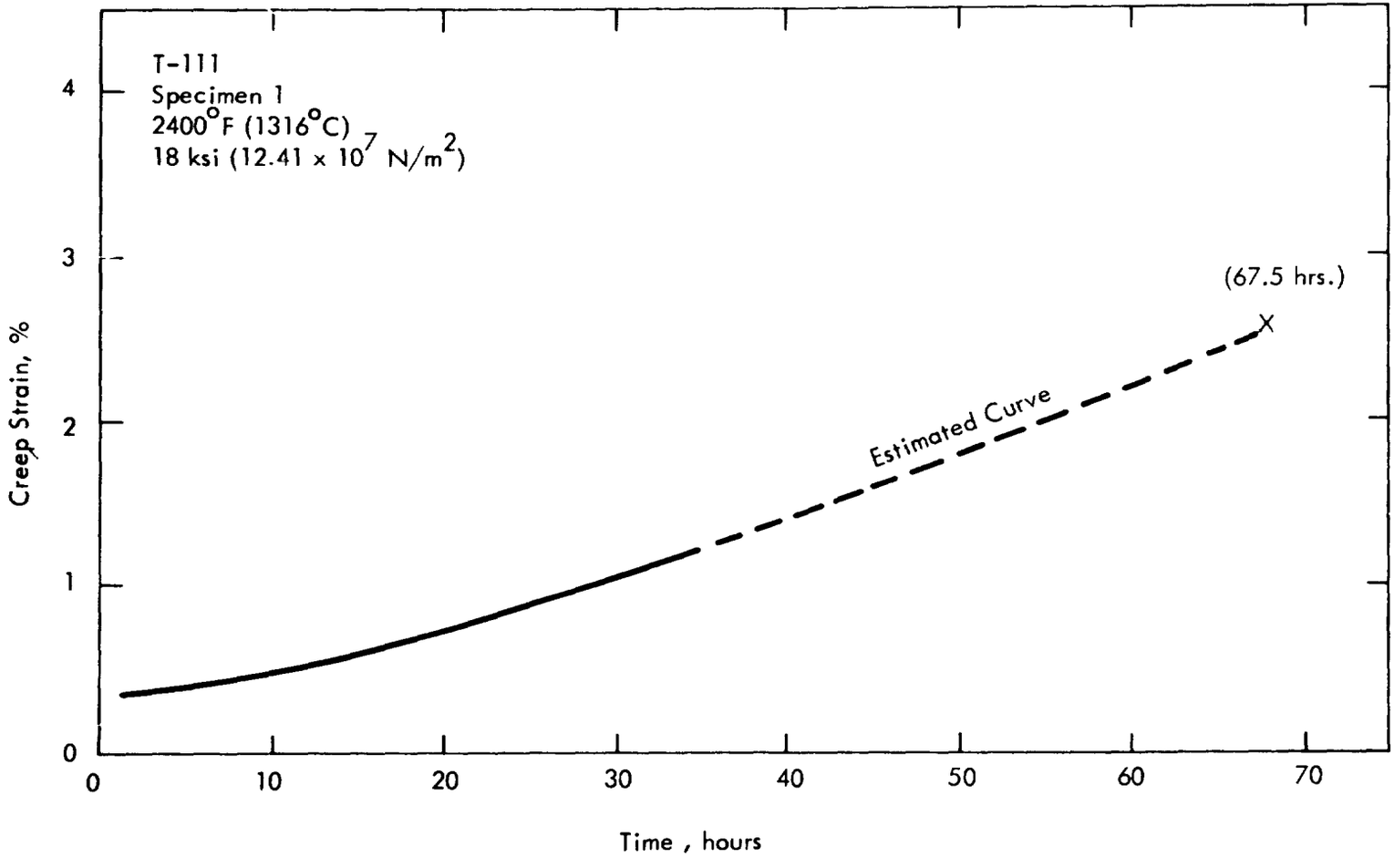

FIGURE 38 - Creep Curve for T-111 Specimen 1.

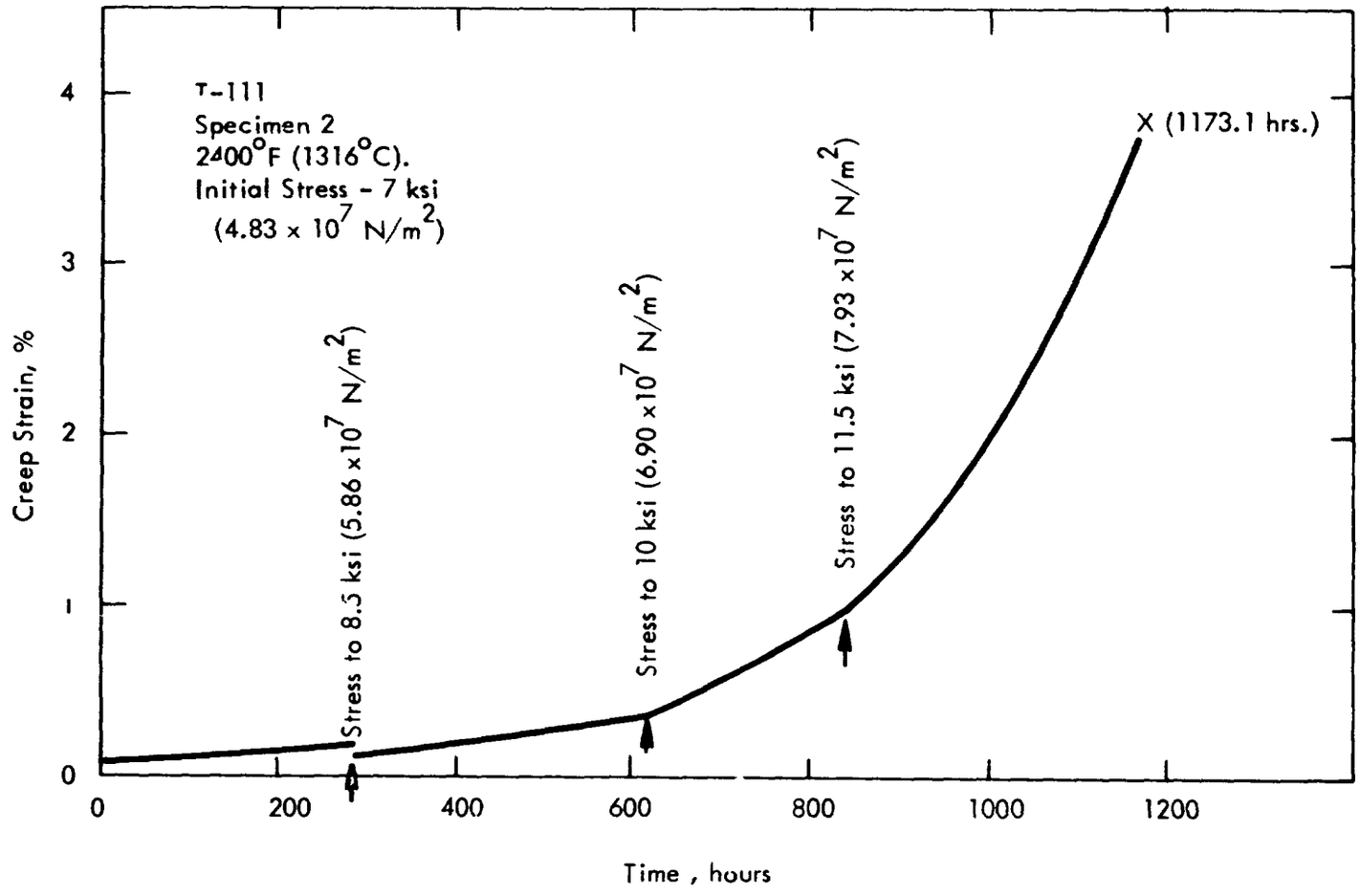

FIGURE 39 - Creep Curve for T-111 Specimen 2.

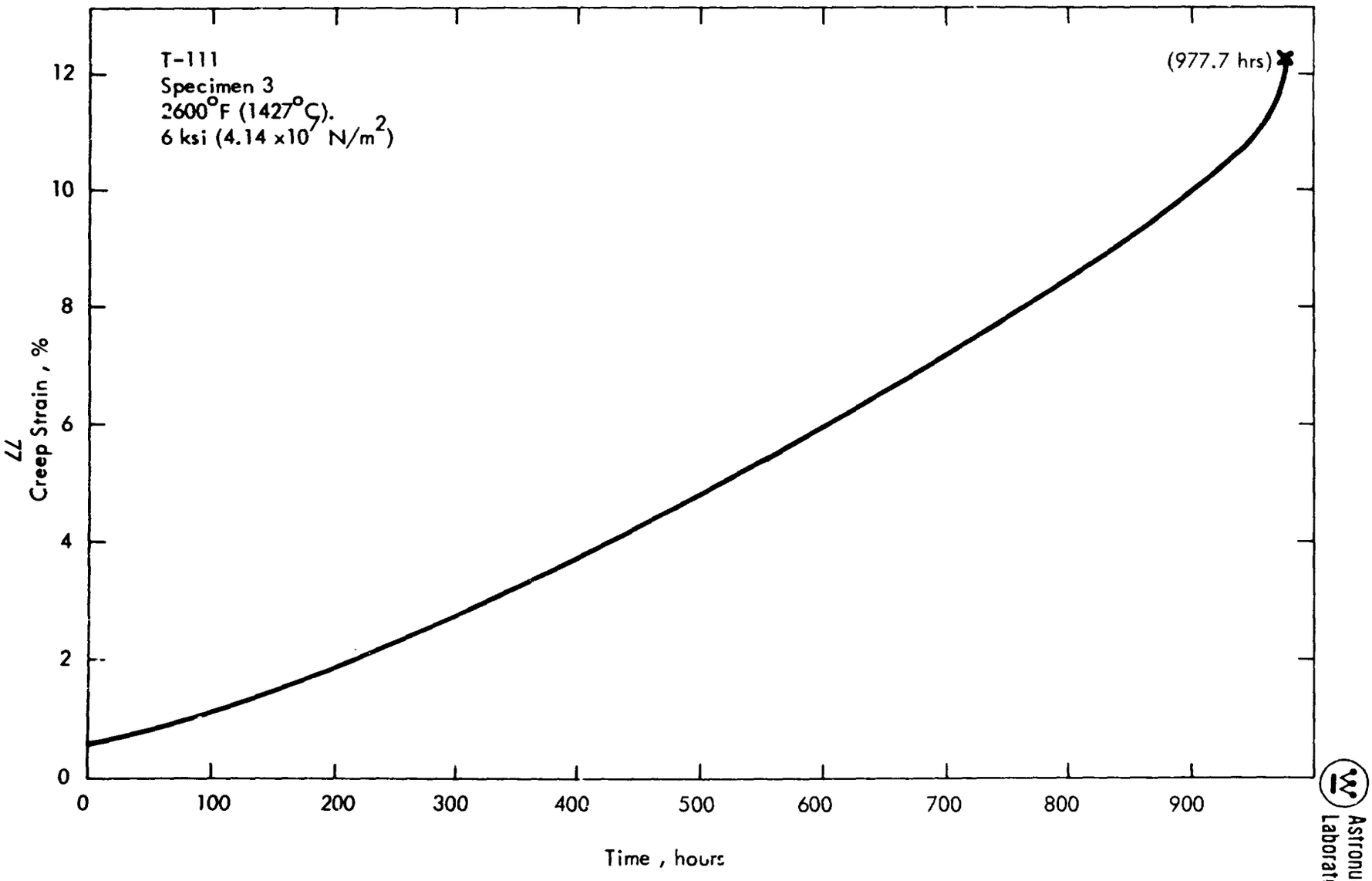

FIGURE 40 - Creep Curve for T-111 Specimen 3.

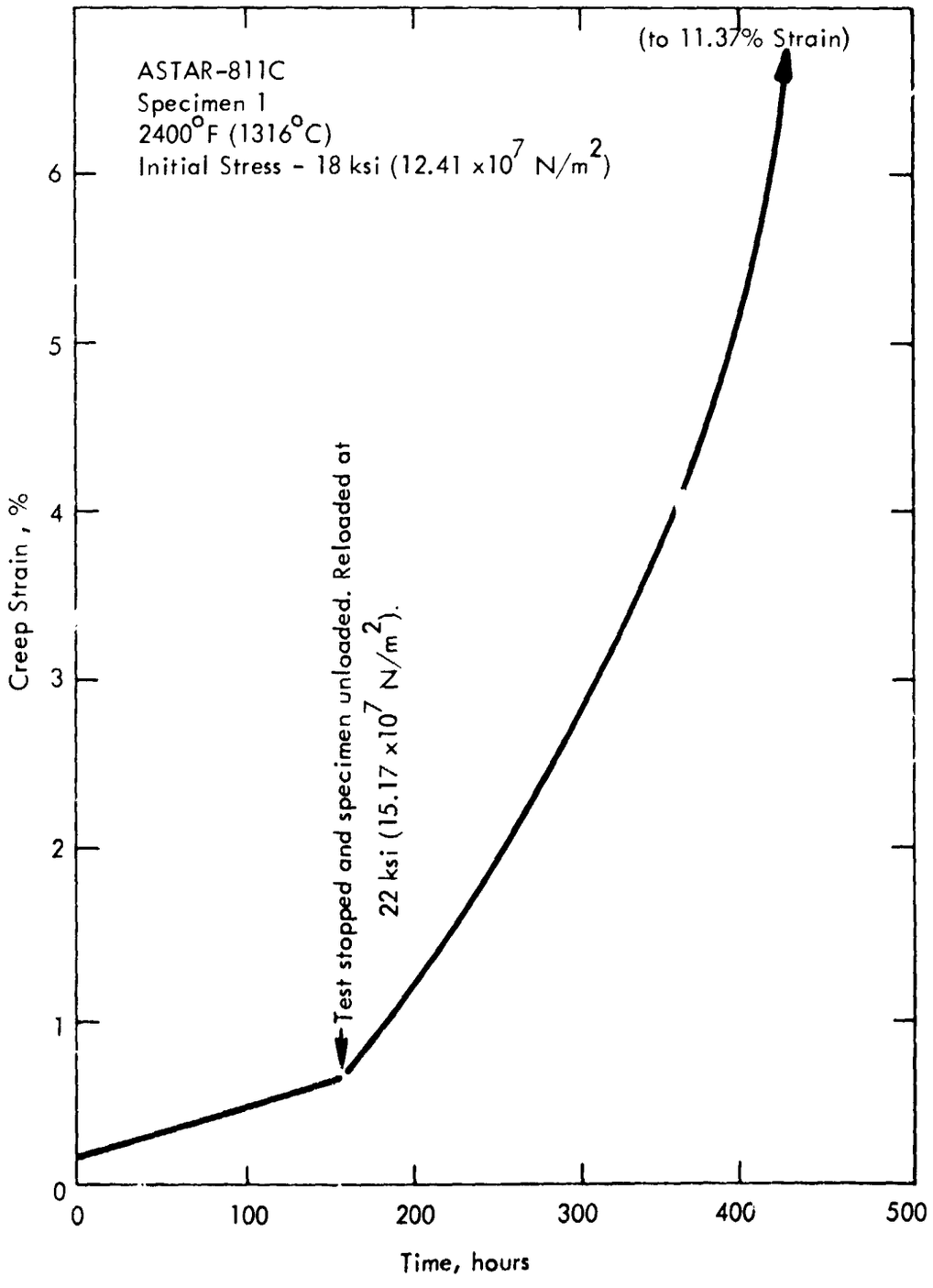

FIGURE 41 - Creep Curve for ASTAR-811C Specimen 1.

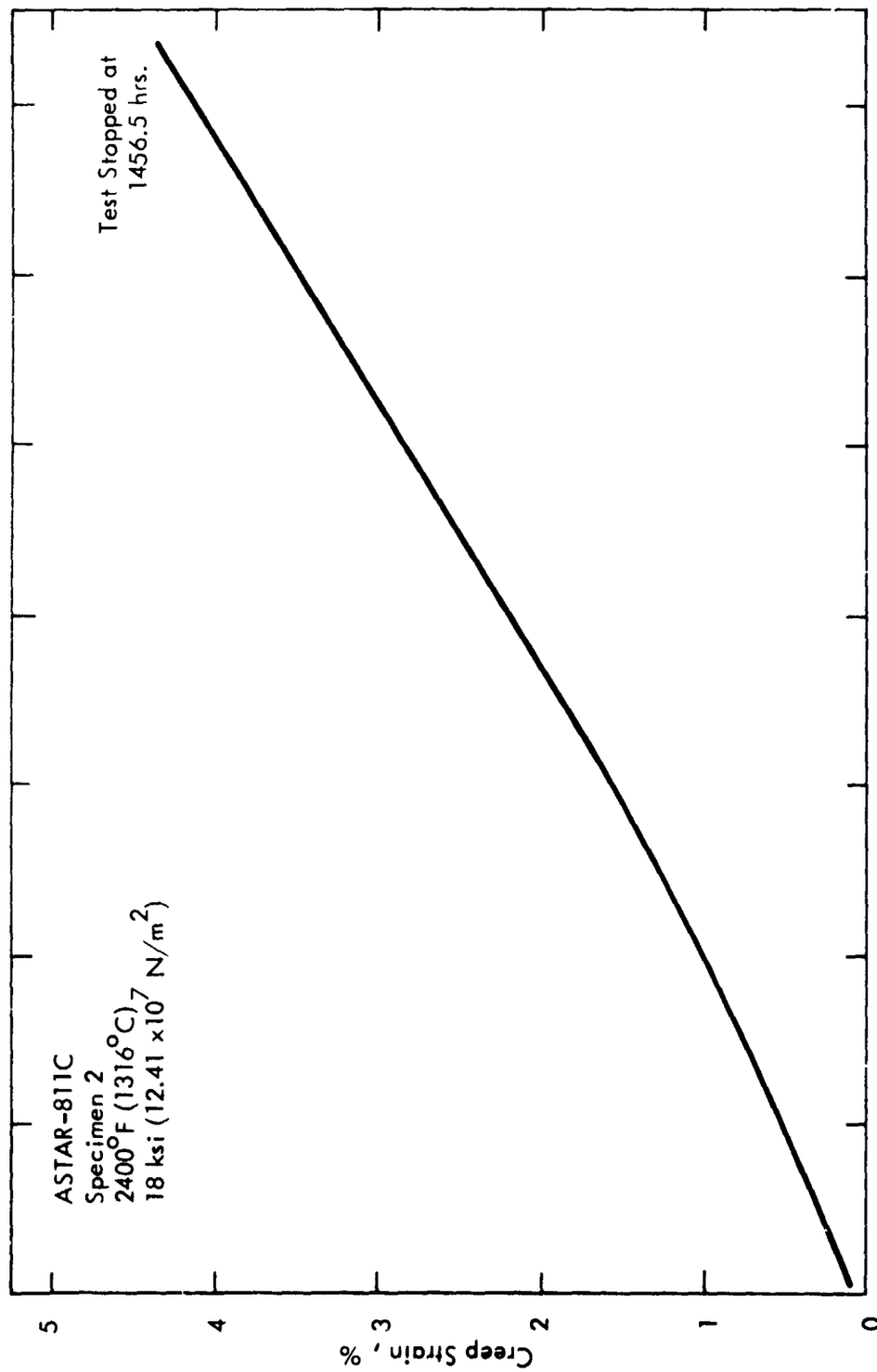

FIGURE 42 - Creep Curve for ASTAR-811C Specimen 2.

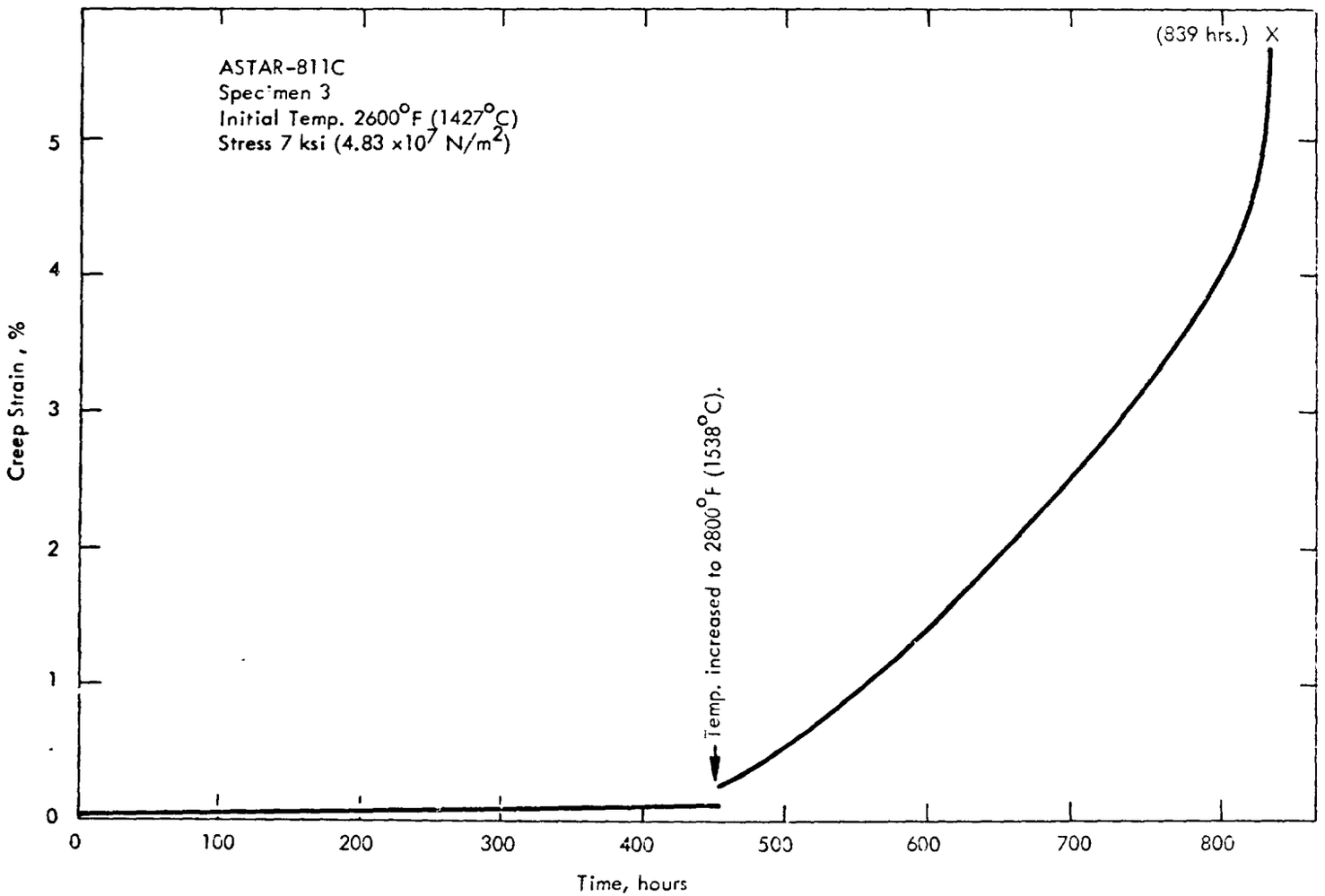

FIGURE 43 - Creep Curve for ASTAR-811C Specimen 3.

Alloy	Spec. No.	Test Temp.		Stress		Time and Corresponding P_{L-M} for 0.5% Strain		
		°F	°C	ksi	10^7 N/m^2	t (hrs.)	P_{L-M}(a)	P_{L-M}(b)
T-111	1	2400	1316	15.0	10.34	21	46.6	25.9
T-111	2	2400	1316	10.0	6.90	180	49.3	27.4
T-111	3	2600	1427	6.0	4.14	80	51.7	28.7
ASTAR-811C	1	2400	1316	18.0	12.41	160	49.3	27.3
ASTAR-811C	2	2400	1316	18.0	12.41	230	49.6	27.5
ASTAR-811C	3	2800	1538	7.0	4.83	80	55.1	30.6

(a) $P_{L-M} = T_{o_R} (15 + \log t(\text{hrs.})) \times 10^{-3}$

(b) $P_{L-M} = T_{o_K} (15 + \log t(\text{hrs.})) \times 10^{-3}$

TABLE 16 - Larson-Miller Parametric Data for Creep of T-111 and ASTAR-811C Longitudinal GTA Sheet Weld Specimens.

23,308 T-111 Specimen 1 50X

Tested at 2400°F (1316°C). Fracture Strain 2.49%.
Annealed 4 hrs- 3600°F(1982°C) Prior to Test.

23,311 ASTAR-811C Specimen 1 100X

Tested at 2400°F (1316°C). Fracture Strain 11.37%.

FIGURE 44 - T-111 and ASTAR-811C GTA Sheet Weld Specimens after Creep Testing as Indicated.

cracking and void formation was extensive throughout the gage lengths of all specimens, being predominantly situated on boundaries transverse to the stress axis. The only evidence of slip which could be seen on the surface after testing was localized in the vicinity of the fracture.

Previous investigations of the creep behavior of ASTAR-811C had indicated the possibility of precipitate redistribution to grain and subgrain boundaries during creep testing[5]. In the present study, however, the pre-test anneal at 1982°C (3600°F) had already resulted in precipitation at subgrain boundaries. No further change in the amount or distribution of precipitates was observed due to testing. A typical post-test microstructure is shown in Figure 45.

One of the purposes of these tests was to try to make some estimate of the contribution of grain boundary sliding to total creep strain by noting grain boundary displacements relative to pre-scribed fiducial lines on the gage section of the specimens. Typical grain boundary-fiducial line intersections are shown in Figure 46. Review of the surfaces of the specimens revealed considerable evidence of grain boundary sliding. From the evidence one must conclude grain boundary sliding is making a "substantial" contribution to the total creep strain. While quantitative techniques have been developed and applied to obtaining numerical values for the contribution of grain boundary sliding[11-15] these techniques require tedious measurements and calculations. Such effort was beyond the scope of the present program.

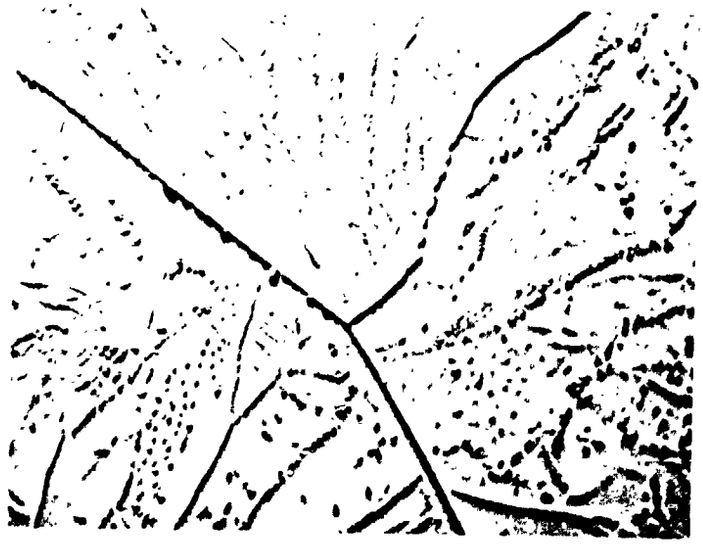

23,312 400X

23,312 ASTAR-811C Specimen 2 750X

Tested at 2400°F (1316°C). Test Stopped at 4.02% Strain.

FIGURE 45 - Post-Test Microstructure of ASTAR-811C GTA Sheet Weld Specimen Tested at 2400°F(1316°C).

ASTAR-811C Specimen 1 400X

After 11.37% Strain. Tested at 2400°F (1316°C).

ASTAR-811C Specimen 3 50X

After 5.47% Strain. Tested at 2600°F (1427°C) and 2800°F (1538°C).

FIGURE 46 - Surface Photographs of ASTAR-811C Sheet Specimens after Creep Testing as Indicated.

5.0 DISCUSSION

The results of the tensile tests on T-111 are summarized in Figure 47 in terms of tensile elongation vs. test temperature. Included for the data on GTA sheet welded material are data from an earlier phase of this program[2]. (A similar graph could be presented for ASTAR-811C but would offer no unique information). The difference in the behavior of the wrought-recrystallized material implied in Figure 47 appears to be due to the very small grain size of those specimens rather than to a basic difference in deformation behavior. Metallographic studies indicated the relative grain boundary and matrix participation in the tensile deformation process to be essentially dictated by test temperature.

Although not totally inclusive of all the results, the data represented in Figure 47 do essentially provide a summary of the significant feature of this program. That is, intergranular failure (not always leading to immediate fracture, however) occurs at low strains during testing at intermediate to high temperatures.

The minimum in the ductility vs. temperature curves of Figure 47 is in no way unique to these alloys and does not reflect a peculiarity of either tantalum-base alloys or body-centered-cubic metals in general. A general discussion of the factors influencing this type of behavior has been presented elsewhere in this program[2]. The conclusions reached included:

- At temperatures below the temperature of minimum or decreased ductility deformation proceeds as the net result of intracrystalline slip; hence, the ductility is high or "normal".
- At higher temperatures, where grain boundary shearing may be a dominant mode of deformation, fissures or cracks appear and grow along grain boundaries until they meet, thereby completing the fracture at low overall elongation. This is the region of minimum or decreased ductility.
- At still higher temperatures softening processes such as recovery and/or recrystallization occur during deformation. The nucleation and growth of new grains (and hence new, crack-free grain boundaries) serves to alleviate the growth of the grain boundary fissures and high ductility is restored.

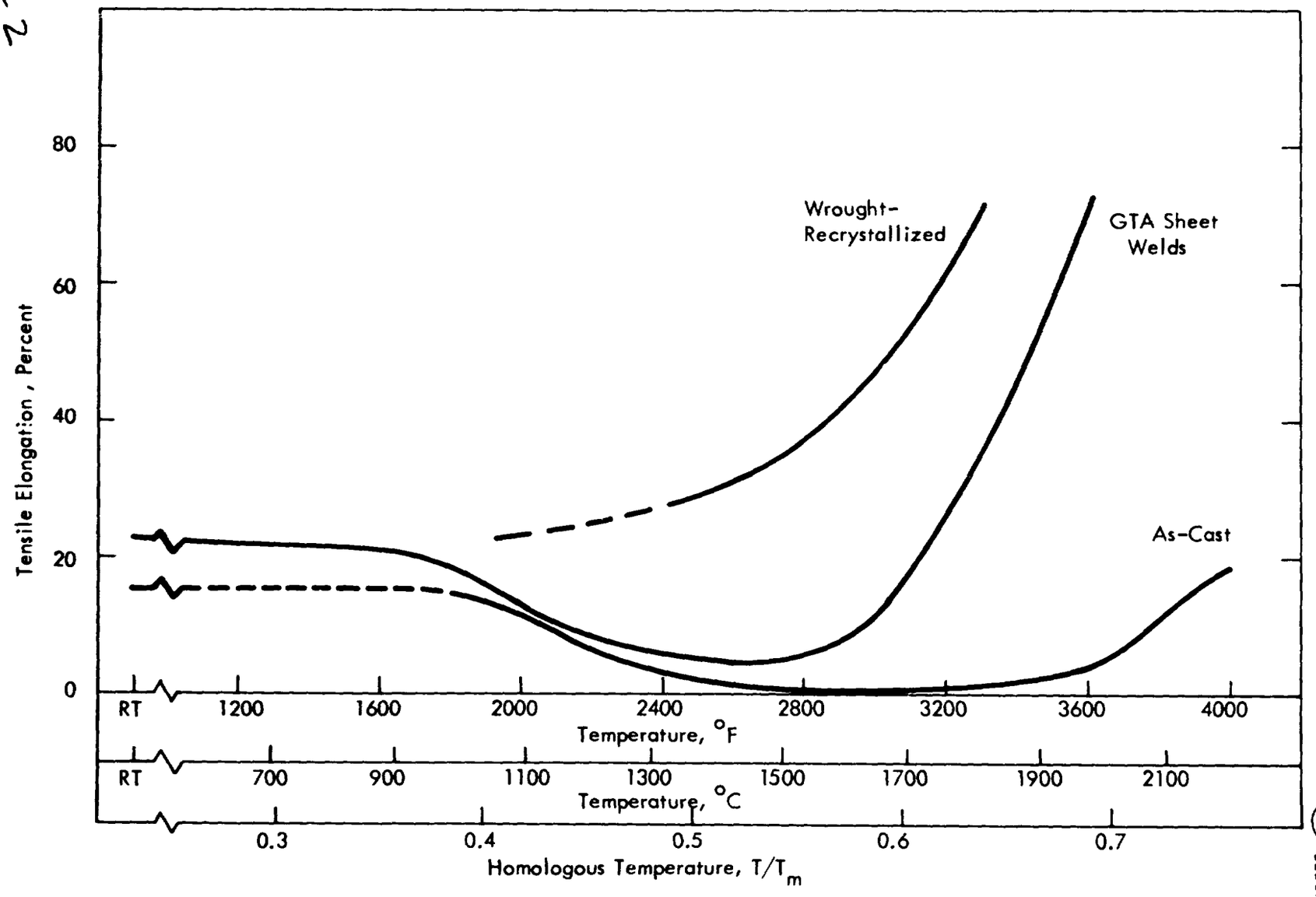

FIGURE 47 - Tensile Elongation vs. Test Temperature for T-111 Alloy Specimens Tested on this Program.

Modifications are of course required to the above arguments in the case of more complex alloys. Nevertheless certain guidelines are established which provide some appreciation of the factors involved.

While the preceding description is phenomenologically accurate, it is not completely satisfying since it provides no rationale which aids in understanding why the transition from transcrystalline to intercrystalline failure occurs. It is important to recall from the photomicrographs and scanning electron micrographs presented in Section 4 of this report that, despite low total strain at failure, considerable, and in many cases extensive, deformation has occurred in a localized grain boundary zone prior to failure. The problem therefore is to try to understand the reasons for the concentration of deformation at the grain boundaries arising from high temperature deformation.

The bulk of experimental evidence, obtained on a wide variety of alloys, indicates that any change in composition or structure which tends to increase the shear strength of the grain volumes, without increasing the shear strength of the grain boundaries, will promote intercrystalline failure. Although in general this applies mainly to deformation under creep conditions the results of this program indicates the same observation can be generalized to the case of tensile deformation, at least for the slower strain rates. This is probably due to the somewhat higher test temperatures used for many of tensile tests relative to those used for creep testing. To rationalize this behavior we can consider, as a function of temperature, the factors known to control the deformation process. Of particular interest to us is the role of grain boundaries in deformation.

The deformation process in metals is greatly influenced by the dislocation mobility and the formation (and stability) of dislocation pileups. These factors depend on both material parameters (crystal structure, grain size and orientation, and the morphology and distribution of second phases) and test parameters (temperature, strain rate and stress). The interrelation of these factors is obvious.

At low and intermediate temperatures ($< 0.5\ T_m$) polycrystalline metals deform essentially by slip deformation within the grains. To maintain continuity of the specimen, each grain deforms in approximately the same manner as the specimen as a whole. However, to maintain continuity of stress throughout the system, the deformation will be inhomogeneous to some degree; i.e. variations will occur from grain to grain and from point to point within a grain. Measurements on specimens deformed at low temperatures have shown deformation to be less in the vicinity of grain boundaries than the average deformation of the grains [16]. The decreased deformation adjacent to the grain boundaries implies the boundaries are a source of strength. This can be understood in terms of the fact the grain boundaries serve as effective barriers to slip dislocations. Hence, at low temperatures dislocation pileups occur and the resulting back stresses serve to strengthen the grain volumes by a work-hardening process. Dislocation mobility considerations are restricted to conservative (glide) motion since climb is not generally possible at temperatures much below $0.5\ T_m$.

As the test temperature is increased the overall behavior is altered due to several factors. First, the formation of stable dislocation pileups is difficult now because of the relative ease with which cross-slip can occur. This is particularly true in body-centered cubic metals with their characteristically high stacking fault energies. Secondly, although deformation probably still originates primarily within the grain volumes, the regions adjacent to the grain boundaries demonstrate a marked reduction in their ability to tolerate shear stresses. This ease of shear deformation results in localized bending or distortion of the grains along the face of the grain boundary. To relax or accommodate this distortion a recovery process such as polygonization has been suggested as likely [17,18]. A schematic illustration of such a process is shown in Figure 48.

It appears therefore that the transition from transcrystalline to intercrystalline fracture at elevated temperatures is the consequence of the combined influence of both factors -- high intragranular dislocation mobility and a decreased resistance to grain boundary shear. While the first of these is relatively easy to explain on the basis of thermally activated dislocation

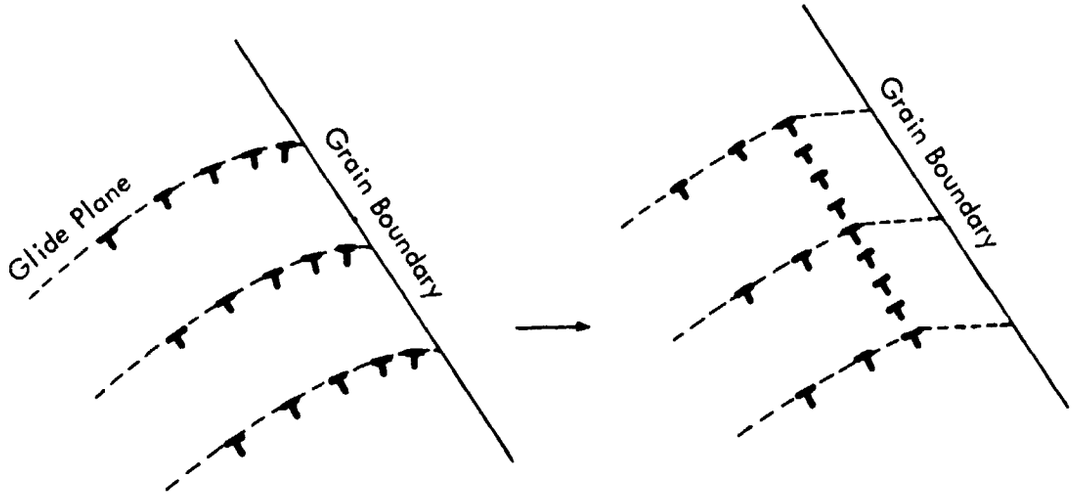

FIGURE 48 - Schematic Illustration Showing Polygonization Occurring in Grain Boundary Region at High Temperatures.

the precise reasons for the latter are not clearly understood. The high atomic mobility which exists at elevated temperatures coupled with the high lattice misfit at the boundaries must certainly play a role but a quantitative understanding will require a more precise knowledge of dislocation-grain boundary interactions at the atomic level.

Translating the above considerations to fit the specific results of this program suggests the following;

- Up to about 1427°C (2600°F) deformation is controlled by intracrystalline slip. Fractures are the result of ductile transgranular shear processes.
- In the approximate temperature range 1538° to 1816°C (2800° to 3300°F), the grain boundary regions deform much more readily than the grain volumes, due to their inability to withstand shear stresses. Hence, the bulk of the deformation occurs along the grain boundary regions and fractures inevitably occur by intercrystalline failure.
- Above about 1982°C (3600°F) the extreme mobility of dislocations and the activation of grain boundary migration and dynamic softening processes mitigates or supersedes the problem of grain boundary shear. As a result the formation and propagation of intercrystalline cracks are much more difficult and ductility again increases.

The differences in behavior of ASTAR-811C and T-111 were mainly observed in the lower range of temperatures -- i.e. below about 1538°C (2800°F) . This suggests that if the carbide precipitates are influencing the deformation process they are doing so mainly by promoting the retention of intracrystalline slip as the primary mode of deformation to temperatures where grain boundary shear is already dominant in the deformation of T-111. Alternatively, this could be due to the presence of grain boundary precipitates in ASTAR-811C which serve to reduce the effective free length of the boundary, thereby reducing the stress concentrations which develop. At least on the scale resolvable by optical metallography the latter does not seem to be true although more positive confirmation would certainly have to be made with more sophisticated techniques such as transmission electron microscopy.

As a final check on the general accuracy and applicability of the picture presented above for the present program, selected T-111 specimens were examined by thin film transmission electron

microscopy. The purpose of this work was to determine the dislocation structure as a function of test temperature. The specimens used for this work included the as-cast specimens tested at 1205°, 1649° and 2205°C (2200°, 3000° and 4000°F). Figure 49 shows typical dislocation distribution within the grain interiors of the specimen tested at 1205°C (2200°F). Extremely dense tangles of dislocations could be seen emanating from the grain boundaries into the grain volumes suggesting the boundary regions are becoming work hardened and are therefore forcing deformation to extend back into the grain volumes.

Testing at 1649°C (3000°F) resulted in the intragranular dislocation structure shown in Figure 50. The dislocation density is less than for the 1205°C (2200°F) specimen and the many closed loops now apparent indicate recovery is occurring during cooling from the test temperature. Some dislocation structure was evident along the grain boundary regions although not nearly as dense as for the 1205°C (2200°F) specimen. The grain volumes appear significantly "harder" than the grain boundary regions indicating the major deformation will be localized at the boundaries.

The specimen tested at 2205°C (4000°F) revealed a very low dislocation density with the structure consisting largely of closed or partly closed loops. A trace of a former grain boundary is shown in Figure 51. Note the fact the surrounding matrix is extremely "clean", which suggests considerable recovery and dislocation annihilation have occurred during the cooldown from the test temperature.

The transmission electron microscopy provided another piece of information of interest. Although T-111 is basically a solid solution alloy, some precipitates are present due to the residual interstitial content of the alloy. A region where the precipitate density was found to be particularly high (in the specimen tested at 1205°C (2200°F) is shown in Figure 52. The blocky precipitates are cubic (NaCl type) and are probably carbides. Note the edges are generally parallel to $\{110\}$ although some of the smaller precipitates have edges parallel to $\{100\}$. From the electron diffraction pattern of the precipitate and the matrix the habit

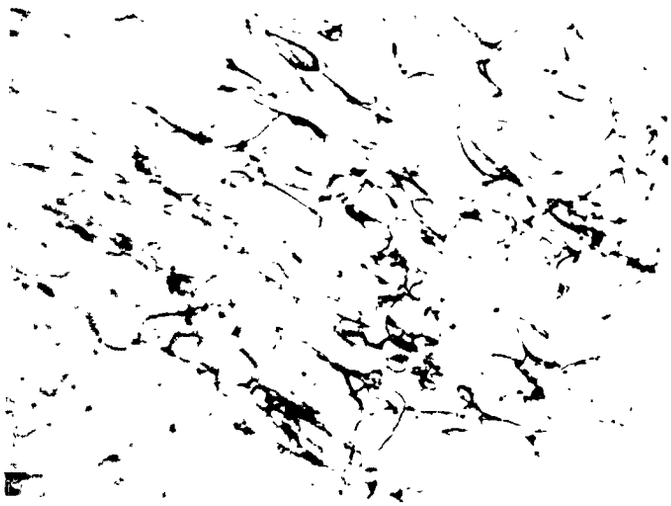

02517 1.0 μm. 26,000X

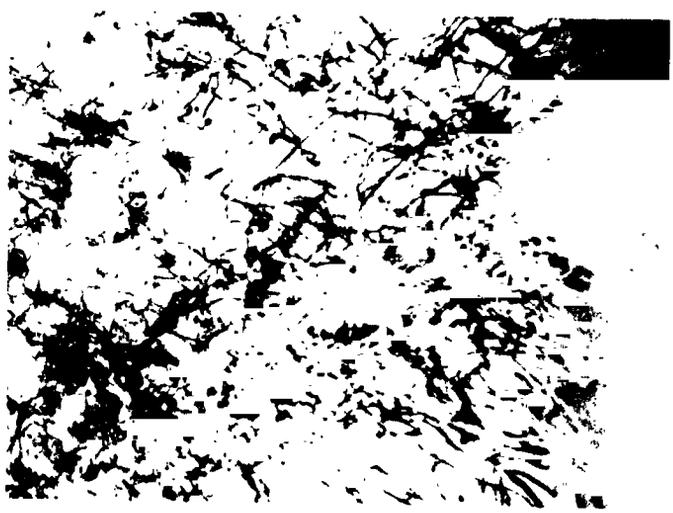

02519 1.0 μm. 26,000 X

Strain Rate 0.005 min^{-1}. Fracture Strain 6.4%.

FIGURE 49 - Transmission Electron Micrographs of an As-Cast T-111 Specimen Tested at 2200°F (1205°C). Typical Dislocation Structure in Grain Interiors.

00042 0.5 μm. 59,000X

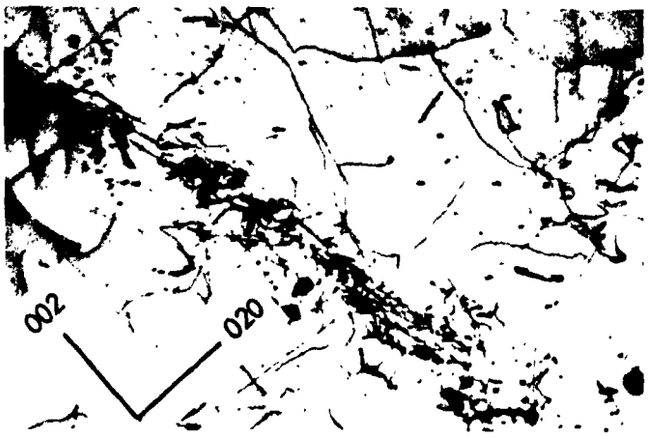

00047 1.0 μm. 25,400X

Strain Rate 0.005 min^{-1}. Fracture Strain 0.1%.

FIGURE 50 - Transmission Electron Micrographs of an As-Cast T-111 Specimen Tested at 3000°F (1649°C). Precipitates and Debris Adjacent to Former Grain Boundary Area.

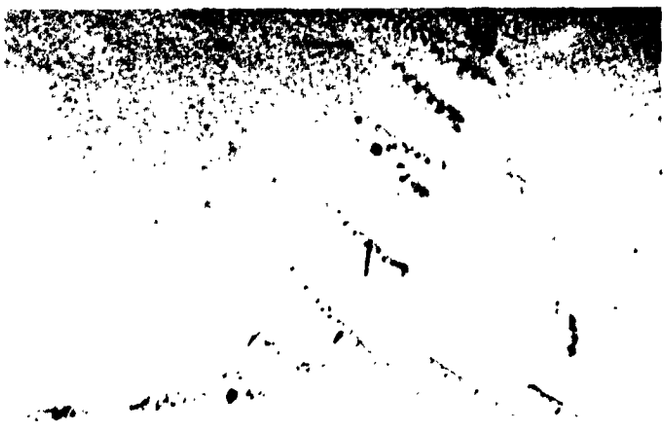

00004 1.0 μm. 36,000X

Strain Rate 0.05 min^{-1}. Fracture Strain 18.3%.

FIGURE 51 - Transmission Electron Micrograph of an As-Cast T-111 Specimen Tested at 4000°F (2205°C). Trace of Former Grain Boundary Shown.

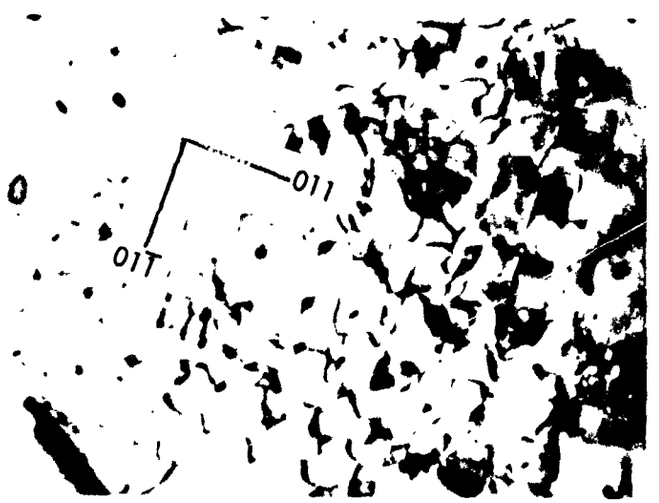

02481 0.3 μm. 81,000X

Strain Rate 0.005 min^{-1}. Fracture Strain 6.4%.

FIGURE 52 - Transmission Electron Micrograph of an As-Cast T-111 Specimen Tested at 2200°F (1205°C). (See text for details of precipitate-matrix habit relationships).

of the precipitate was found to be ;

$$\{100\}_p \;//\; \{100\}_m$$

$$[100]_p \;//\; [011]_m$$

$$[110]_p \;//\; [010]_m$$

where the subscripts p and m refer to precipitate and matrix, respectively. These results agree with those predicted for face-centered cubic precinitates in a body-centered cubic matrix when there is small lattice mismatch [19]. The lattice mismatch was estimated as approximately 8%.

The results of the transmission electron microscopy are therefore in agreement with those anticipated from more theoretical considerations. We can therefore conclude the transition from intracrystalline to intercrystalline failure is a direct consequence of ;

a - the inability of the grain boundary regions to harden under deformation to withstand large shear stresses without deforming catastrophically, and,

b - the difficulty of establishing stable dislocation pileups and tangle which might serve to work harden the matrix equivalently.

It is to these two factors that any solution of the problem of premature intergranular failure must be addressed.

6.0 CONCLUSIONS

1. A region of reduced ductility, in terms of tensile elongation, exists for T-111 and ASTAR-811C between 1538° and 1816°C (2800° and 3300°F). In this temperature range fractures are intergranular occurring at low total strains.
2. The observed behavior can be rationalized on the basis of a change in the controlling deformation mode. At low temperatures intracrystalline slip and associated work-hardening processes dominate whereas in the critical temperature range grain boundary shear dominates with the result most of the strain is accommodated at the grain boundaries. At very high temperatures dynamic softening processes and other accommodation processes occur preventing the nucleation and growth of intergranular cracks.
3. Increases in grain size, by reducing the total available grain boundary area, aggravate the problem. Hence, the propensity for intergranular failure is highest for very coarse grained as-cast material and less for fine grained wrought-recrystallized specimens.
4. Differences in the behavior of ASTAR-811C and T-111 were for the most part confined to the lower range of temperatures where ASTAR-811C retained a higher degree of "ductility" to slightly higher temperatures than T-111.
5. Scanning electron microscopy performed directly on the as-fractured specimens indicated that even for the cases where tensile elongation was virtually nil considerable deformation had occurred on a very localized scale prior to fracture.
6. Grain boundary sliding was found to contribute substantially to the total strain during creep testing at 1316° to 1538°C (2400° to 2800°F) although quantitative estimates of the contribution could not be made.
7. Transmission electron microscopy, performed on as-cast T-111 specimens tested at 1205°, 1649° and 2205°C (2200°, 3000° and 4000°F) revealed dislocation structures in agreement with those qualitatively predicted from more basic considerations.

7.0 REFERENCES

1. Stoner, D. R. and Buckman, R. W., Jr. ,"Development of Large Diameter T-111 Tubing", NASA CR-72869, December, 1970.

2. Gold, R.E. and Lessmann, G.G. , "Influence of Restraint and Thermal Exposure on Welds in T-111 and ASTAR-811C" , NASA CR-72858 , January, 1971 .

3. Lessmann, G.G. and Gold, R.E. , "The Varestraint Test for Refractory Metals", NASA CR-72828 , November, 1970 .

4. Buckman, R.W., Jr. and Goodspeed, R.C., "Development of Precipitation Strengthened Tantalum Base Alloy, ASTAR-811C" , Work done under Contract NAS 3-2542, Summary Topical Report, WANL-PR-(Q)-016 , (1968).

5. Buckman, R.W., Jr., and Goodspeed, R.C., "Development of Precipitation Strengthened Tantalum Base Alloys ", Final Report on Contract NAS-2542, WANL-PR-(Q)-017, NASA CR-1642 , May ,1971.

6. Adams, C.M., Jr. ,"Cooling Rates and Peak Temperatures in Fusion Welding", Welding Journal , Research Supplement, 37 (5), pp. 210-s to 215-s , (1958).

7. Rosenthal, D., "Mathematical Theory of Heat Distribution During Cutting and Welding", Welding Journal, Research Supplement, 20 (5), pp. 220-s to 234-s , (1941).

8. Weiss, S. , Ramsey, J.N. and Udin, H., "Evaluation of Weld Cracking Tests on Armor Steel", Welding Journal , Research Supplement, 35 (7), pp. 348-s to 356-s , (1956).

9. Low, J. R. , Jr. , The Fracture of Metals , Progress in Materials Science, Vol. 12, No.1. (1963).

10. Lessmann, G.G. , Gold, R.E. , Arcella, F.G. and Reed, F. ,"Material Considerations for Design of the Potassium Turboalternator (KTA) ", WANL-TME-1889, January,1969.

11. Rachinger, W.A., J. Inst. of Metals, 81 , p.33 (1952).

12. Ishida, Y. , Mullendore, A. W. , and Grant, N.J., Trans AIME, 230 , p.1454 (1964).

13. Bell, R,L. and Graeme-Barber, C. , Jnl. of Materials Science, 5 , p. 933 (1970) .

14. McLean, D., J. Inst. of Metals, 81 , p. 133 (1952).

15. Stevens, R. N. , Trans AIME , 236 , p. 1762 (1966).

16. Urie, V.M. and Wain, H. L. , J. Inst. of Metals, 81 , p.153 (1952-1953).

17. Crussard, C. and Friedel, J. ," Theory of Accelerated Creep and Rupture" in Creep and Fracture of Metals at High Temperatures , London , HMSO (1956) , pp. 243-262.

18. Rhines, F. N. ,"Mechanism of Grain Boundary Displacement and Its Relation to the Creep Process as a Whole ", in Creep and Fracture of Metals at High Temperatures , London, HMSO (1956) , pp. 48-57.

19. Ryan, N. E. , Soffa, W. A.and Crawford, R. C. , Metallography, 1 , No. 2 , pp. 195-220 (1968).